Stem Cell Reports
Article

OPEN ACCESS

Contribution of ATOH1$^+$ Cells to the Homeostasis, Repair, and Tumorigenesis of the Colonic Epithelium

Fumiaki Ishibashi,[1] Hiromichi Shimizu,[1,4] Toru Nakata,[1] Satoru Fujii,[1] Kohei Suzuki,[1] Ami Kawamoto,[1] Sho Anzai,[1] Reiko Kuno,[1] Sayaka Nagata,[1] Go Ito,[1,5] Tatsuro Murano,[1] Tomohiro Mizutani,[1] Shigeru Oshima,[1] Kiichiro Tsuchiya,[1] Tetsuya Nakamura,[2] Mamoru Watanabe,[1] and Ryuichi Okamoto[1,3,*]

[1]Department of Gastroenterology and Hepatology
[2]Department of Advanced Therapeutics in GI Diseases
Graduate School, Tokyo Medical and Dental University, Tokyo 113-8519, Japan
[3]Center for Stem Cell and Regenerative Medicine, Graduate School, Tokyo Medical and Dental University, 1-5-45 Yushima, Bunkyo-ku, Tokyo 113-8519, Japan
[4]Department of Medicine, University of California, San Francisco, San Francisco, CA 94143, USA
[5]Institute of Clinical Molecular Biology, Christian-Albrechts-University Kiel, 24118 Kiel, Germany
*Correspondence: rokamoto.gast@tmd.ac.jp
https://doi.org/10.1016/j.stemcr.2017.11.006

SUMMARY

ATOH1 is a master transcription factor for the secretory lineage differentiation of intestinal epithelial cells (IECs). However, the comprehensive contribution of ATOH1$^+$ secretory lineage IECs to the homeostasis, repair, and tumorigenesis of the intestinal epithelium remains uncertain. Through our ATOH1$^+$ cell-lineage tracing, we show here that a definite number of ATOH1$^+$ IECs retain stem cell properties and can form ATOH1$^+$IEC-derived clonal ribbons (ATOH1$^+$ICRs) under completely homeostatic conditions. Interestingly, colonic ATOH1$^+$ IECs appeared to exhibit their stem cell function more frequently compared with those of the small intestine. Consistently, the formation of ATOH1$^+$ICRs was significantly enhanced upon dextran sodium sulfate colitis-induced mucosal damage. In addition, colonic ATOH1$^+$ IECs acquired tumor stem cell-like properties in the azoxymethane-DSS tumor model. Our results reveal an unexpected contribution of colonic ATOH1$^+$ IECs to maintaining the stem cell population under both homeostatic and pathologic conditions and further illustrate the high plasticity of the crypt-intrinsic stem cell hierarchy.

INTRODUCTION

The intestinal epithelium is maintained by intestinal stem cells (ISCs), which reside at the bottom of the crypt (Okamoto and Watanabe, 2016). ISCs are identified by the expression of specific genes, such as leucine-rich repeat-containing G-protein-coupled receptor 5 (*Lgr5*) (Barker et al., 2007). The differentiation of intestinal epithelial cells (IECs) predominantly proceeds in a unidirectional manner, starting from the ISCs to the terminally differentiated cells. In the earliest phase of this process, progenitor cells are committed either to a secretory or absorptive lineage based on the expression of key transcription factors such as atonal homolog-1 (ATOH1) or hairy and enhancer of split-1 (HES1) (Jensen et al., 2000; Yang et al., 2001).

However, a recent study showed that small-intestinal IECs committed to the absorptive lineage can exhibit ISC-oriented de-differentiation upon severe epithelial damage (Tetteh et al., 2016). Other studies have further highlighted the plasticity and ISC-oriented de-differentiation of secretory lineage-committed IECs in the small intestine, which are identified by the expression of NGN3 (Schonhoff et al., 2004), Delta-like 1 (DLL1) (van Es et al., 2012), and doublecortin-like kinase 1 (DCLK1) (Westphalen et al., 2014). ATOH1$^+$ label-retaining cells (LRCs) reside at the +4 position and serve as secretory progenitor cells, but they can also exhibit ISC properties upon severe tissue injury (Buczacki et al., 2013). These studies indicated that a collective proportion of ATOH1$^+$ secretory lineage-committed IECs retain their potential to revert to ISCs and can exhibit ISC-specific properties upon severe tissue injury to compensate for the massive loss of genuine ISCs (Mills and Sansom, 2015). Consistent with this finding, a recent single-cell analysis of LGR5$^+$ IECs identified the rare presence of ATOH1$^+$LGR5$^+$ double-positive cells in normal small-intestinal crypts (Kim et al., 2016). However, the comprehensive and dynamic contributions of these ATOH1$^+$ potential ISCs under normal and pathologic conditions have yet to be described. In addition, the key factors that can recruit a specific subset of ATOH1$^+$ IECs back to the ISC pool upon severe epithelial damage remain mostly uncertain.

In intestinal tumorigenesis, several studies have shown that LGR5$^+$ ISCs are the cells of origin of sporadic adenomatous polyposis coli (*Apc*)-deficient tumors (bottom-up model) (Barker et al., 2009). Other studies have shown that villus cells can initiate tumor development through overexpression of GREM1 or constitutive activation of the nuclear factor kappa-B (NF-κB) pathway (Davis et al., 2015; Schwitalla et al., 2013). These studies raise the possibility that de-differentiation of lineage-committed IECs may constitute another pathway of intestinal

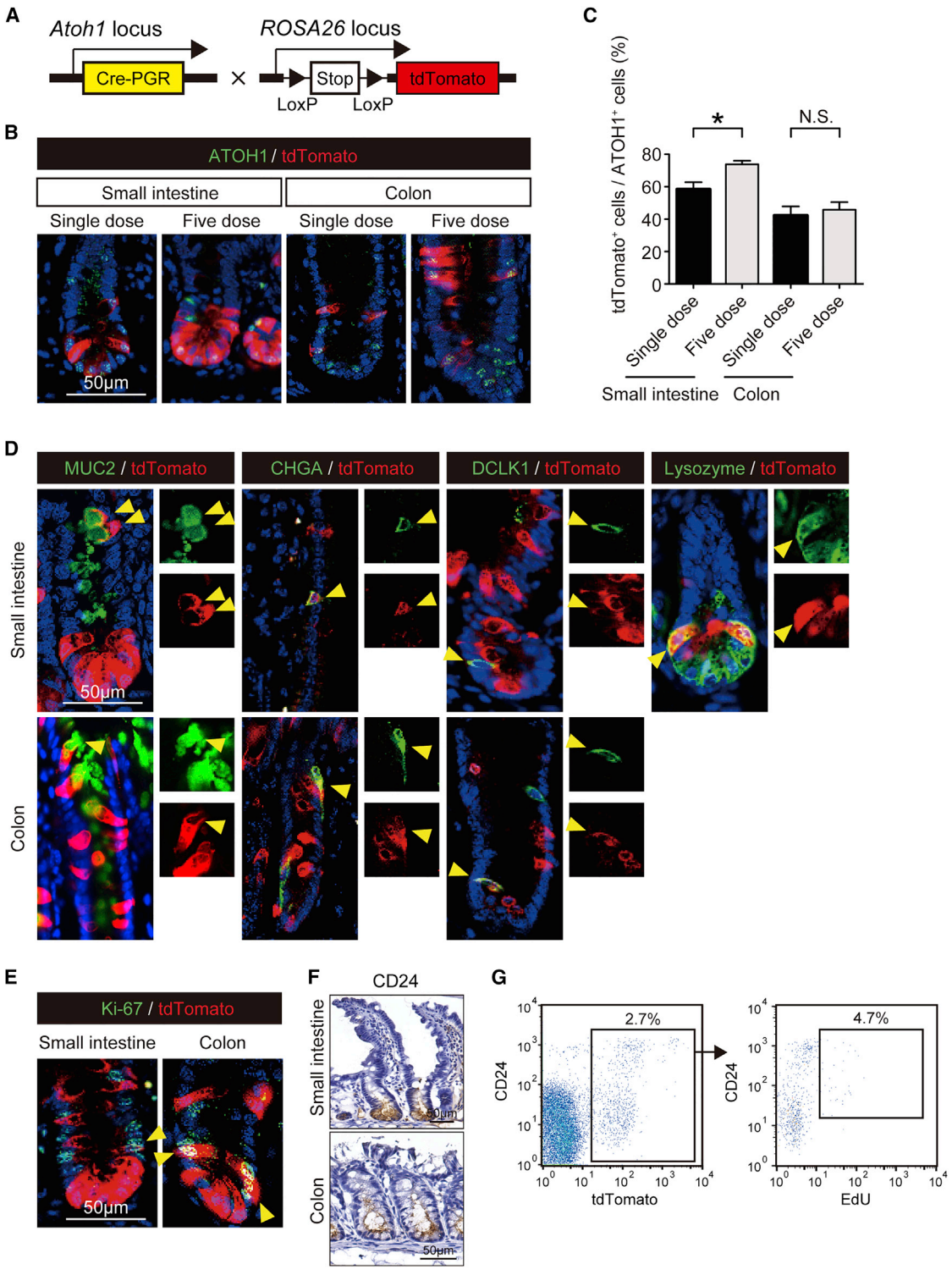

Figure 1. Establishment of ATOH1$^+$ Cell-Lineage Tracing

(A) Schematic representation of the alleles used to establish the *Atoh1*^{tdTomato} mice.

(B) Co-staining of ATOH1 (green) and tdTomato (red) in small-intestinal and colonic tissues. *Atoh1*^{tdTomato} mice were administered RU486 in either a single dose (single dose) or for 5 consecutive days (five-dose) and were then analyzed on the day following the final treatment. Note that all of the tdTomato$^+$ IECs co-expressed ATOH1.

(legend continued on next page)

tumorigenesis (top-down model). Accordingly, inflammatory bowel disease (IBD) patients develop colitis-associated cancers (CACs) via a pathway distinct from that of sporadic colon cancers. Established CACs are abundant in Atoh1$^+$ cells and, thus, retain features of secretory lineage-committed cells, such as mucin production (Park et al., 2006). The robust expression of ATOH1 in CACs may be supported by environmental tumor necrosis factor alpha (TNF-α) and contributes to maintaining their highly malignant properties (Fukushima et al., 2015). However, the potential contribution of ATOH1$^+$ secretory lineage-committed IECs as the origin of CAC tumor stem cells has yet to be described.

In this study, using the ATOH1$^+$ cell-lineage-tracing model, we showed that colonic ATOH1$^+$ IECs could give rise to functional ISCs under both homeostatic and pathologic conditions. The results highlight the unexpectedly broad contribution of ATOH1$^+$ IEC-derived ISCs to the maintenance, regeneration, and progression of colitis-associated tumorigenesis in the colonic epithelium.

RESULTS

Lineage Tracing of ATOH1$^+$ IECs Labels Secretory Lineage IECs

To elucidate the dynamic contribution of ATOH1$^+$ IECs to the maintenance of the intestinal epithelium, we planned a lineage-tracing experiment. Here, we crossed *Atoh1*$^{Cre\text{-}PGR}$ mice (Rose et al., 2009) with *Rosa26-LSL-tdTomato* reporter mice to generate *Atoh1*$^{Cre\text{-}PGR}$*; Rosa26-LSL-tdTomato* mice (*Atoh1*^{tdTomato} mice, Figure 1A). In these mice, the effect of haploinsufficiency due to the knockin allele could not be observed, as confirmed through the analysis of *Atoh1* mRNA and protein expression in the small intestine and colon (Figures S1A–S1C). To optimize the RU486-mediated tdTomato labeling of ATOH1$^+$ IECs, we compared the labeling efficiency between a single dose of RU486 and the injection of RU486 for 5 consecutive days. Both protocols successfully labeled ATOH1$^+$ IECs in the crypts of the small intestine and colon (Figure 1B). The 5-dose protocol resulted in a higher labeling efficiency (Figure 1C) and was therefore employed in the majority of the following experiments.

The analysis performed 24 hr after a single dose of RU486 showed that all secretory lineage IECs and some Ki-67$^+$ IECs were initially labeled by tdTomato (Figures 1D and 1E). Conversely, all of the tdTomato$^+$ IECs were completely negative for HES1 (Figure S1D) and for other absorptive lineage markers (Figure S1E). To further confirm the labeling of mitotic IECs, the uptake of 5-ethynyl-2′-deoxyuridine (EdU) was examined in ATOH1$^+$ IECs. Using CD24 as a marker for lower crypt IECs (Figure 1F) (Sato et al., 2012), we found that 4.7% of the CD24$^{high/mid}$ tdTomato$^+$ IECs were also positive for EdU (Figure 1G).

These results collectively confirmed that our ATOH1$^+$ IEC lineage-tracing system initially labeled both post-mitotic and mitotic secretory lineage-committed IECs in a highly specific manner.

Atoh1$^+$IECs that Retain an ISC-like Phenotype Exist within Normal Intestinal Crypts

LGR5$^+$ ISCs are located at the bottom of the crypt between Paneth cells (Barker et al., 2007). To determine whether any LGR5$^+$ ISCs were labeled by our lineage-tracing system, we crossed our *Atoh1*^{tdTomato} mice with *Lgr5-EGFP-IRES-creERT2* mice to generate *Lgr5-EGFP-IRES-creERT2; Atoh1*$^{Cre\text{-}PGR}$*; Rosa26-LSL-tdTomato* mice (*Lgr5*^{EGFP}*Atoh1*^{tdTomato} mice). The induction of *Atoh1*$^{Cre\text{-}PGR}$ allele-dependent tdTomato labeling in *Lgr5*^{EGFP}*Atoh1*^{tdTomato} mice showed that the tdTomato$^+$ IECs were clearly distinct from LGR5$^+$ ISCs (Figure 2A). However, flow cytometric analysis of ATOH1$^+$ IECs revealed a rare population of LGR5-EGFP$^+$ ATOH1$^+$ double-positive IECs in the small intestine of *Lgr5*^{EGFP}*Atoh1*^{tdTomato} mice (Figure 2B). Consistently, RNAscope *in situ* hybridization (RNAscope ISH) clearly exhibited *Lgr5*$^+$*Atoh1*$^+$ double-positive cells, most frequently at the +4 position or +3 position of the small intestine and colon, respectively (Figure 2C). The integrity of our RNAscope analysis was validated by using positive control tissues (Figures S2A and S2B). Also, tdTomato$^+$ crypt cells co-expressing *Ascl2* were found in both regions (Figure 2D).

CD24 is commonly expressed by small-intestinal and colonic crypt IECs (Figure 1F) and therefore used to identify and isolate LGR5$^+$ ISCs or Paneth cells (von Furstenberg et al., 2011). Our analysis of the CD24^{high}, CD24^{mid}, and

(C) Quantification of ATOH1$^+$ IEC labeling efficiency based on the analysis shown in (B). Data are expressed as the mean ± SEM of biological replicates (n = 3). *p < 0.05, N.S., not significant.
(D) Co-staining of secretory IEC markers (green) and tdTomato (red). tdTomato-labeled MUC2$^+$ goblet cells, CHGA$^+$ enteroendocrine cells, DCLK1$^+$ tuft cells, and Lysozyme$^+$ Paneth cells are shown (yellow arrowheads).
(E) Co-staining for Ki-67 (green) and tdTomato (red) revealed tdTomato$^+$ Ki-67$^+$ double-positive IECs (yellow arrowheads).
(F) Immunostaining of CD24 using small-intestinal and colonic tissue of a wild-type mice.
(G) Representative flow plots of the small-intestinal IECs recovered from the *Atoh1*^{tdTomato} mice on the day after completion of the five-dose RU486 treatment and EdU labeling. The CD24$^{high/mid}$ tdTomato$^+$ fraction (combined population of CD24^{high} and CD24^{mid} cells) was further analyzed based on EdU labeling (right).
See also Figure S1.

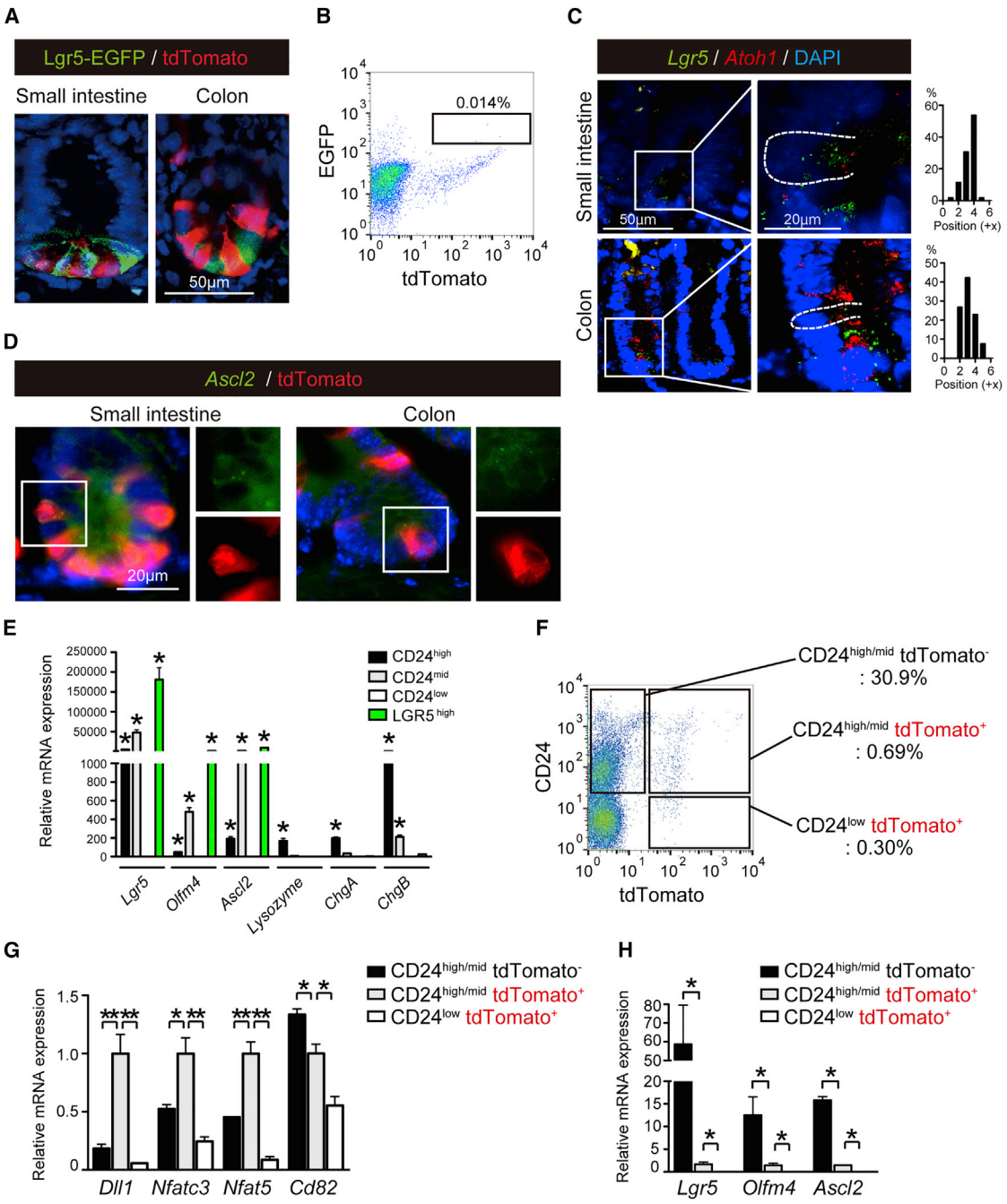

Figure 2. ATOH1^{+} IECs Include a Cell Population that Retains the Expression of Stem Cell-Specific Genes

(A) Co-staining of Lgr5-EGFP (green) and tdTomato (red) in the small-intestinal and colonic crypts of *Lgr5^{EGFP}Atoh1^{tdTomato}* mice on the day following the completion of the five-dose RU486 treatment.

(B) Representative flow plots of the small-intestinal IECs recovered from the *Lgr5^{EGFP}Atoh1^{tdTomato}* mice on the day following the completion of the five-dose RU486 treatment.

(C) RNAscope *in situ* hybridization (RNAscope ISH) for Lgr5 (green) and Atoh1 (red) in the small-intestinal and colonic crypts of wild-type mice. The white dotted line shows the cell margin of a *Lgr5^{+}Atoh1^{+}* double-positive cell. Position number of *Lgr5^{+}Atoh1^{+}* double-positive cells (n = 30 of three independent experiments for each analysis) within a crypt was determined based on its relative position from the bottom of the crypt. Images of the colon are re-used in Figure 4C.

(legend continued on next page)

$CD24^{low}$ fraction of small-intestinal IECs confirmed that the $CD24^{high}$ and $CD24^{mid}$ population includes $LGR5^+$ ISCs, Paneth cells, and enteroendocrine cells (Figure 2E). In contrast, the $CD24^{low}$ population did not include these cell populations. Therefore, the combined population of $CD24^{high}$ and $CD24^{mid}$ small-intestinal IECs ($CD24^{high/mid}$) was collected from the *Atoh1*^{tdTomato} mice on the day after the administration of a single dose of RU486 and sorted into $tdTomato^+$ and $tdTomato^-$ cell fractions (Figure 2F). qRT-PCR analysis of these cell populations showed that gene markers for secretory cell progenitors (*Dll1*) and genes recently identified as markers of LRCs (*Nfatc3*, *Nfat5*) (Buczacki et al., 2013) were highly expressed in the $CD24^{high/mid}$ $tdTomato^+$ IECs (Figure 2G). Exceptionally, CD82 showed highest expression in $CD24^{high/mid}tdTomato^-$ IECs, indicating its preferential expression in the $Atoh1^-$ IEC population. In addition, ISC markers such as *Lgr5, Olfm4*, and *Ascl2* presented the highest expression in the $CD24^{high/mid}tdTomato^-$ population (Figure 2H). However, expression of these genes was also detected in the $CD24^{high/mid}tdTomato^+$ IEC population, although at a much lower level. These results sufficiently indicated that $ATOH1^+$ IECs in the normal intestinal epithelium consist of a heterogeneous cell population, including secretory lineage progenitor cells, and a small population of IECs retaining ISC-specific gene expression.

$Atoh1^+$ IECs Constitutively Exhibit ISC Properties under Homeostatic Conditions

To identify the possible contribution of $ATOH1^+$ IECs as potential ISCs, the dynamic changes in the $tdTomato^+$ IEC distribution were traced for up to 20 days. On day 6, $tdTomato^+$ IECs were found both in the crypts and in the villi, showing mostly a scattered distribution pattern (Figure 3A). At a later phase, the overall number of $tdTomato^+$ IECs showed a clear decrease, indicating that most of these cells exhibit only a short lifetime. However, we found clusters of $tdTomato^+$ IECs in both the small intestine and the colon on day 13 and day 20 (Figure 3A). These $tdTomato^+$ IEC clusters clearly formed a continuous array of IECs along the crypt-villus axis, indicating that they represent clones of IECs arising from a common $ATOH1^+$ IEC-derived ISC origin. Thus, we would like to designate these clusters of IECs as $ATOH1^+$ IEC-derived clonal ribbons ($ATOH1^+$ICRs), representing crypts dominated by $ATOH1^+$ IEC-derived ISCs. The incidence of $ATOH1^+$ICR generation was higher in the colon than in the small intestine, reaching up to 1.0 ribbon per 1,000 crypts (Figure 3B). No $ATOH1^+$ICR formation was found by RU486 treatment in mice carrying *Rosa26-LSL-tdTomato* allele alone (*Null*^{tdtomato}) or by vehicle-alone treatment in *Atoh1*^{tdTomato} mice. Compared with the previous lineage tracing of small-intestinal $DLL1^+$ IECs (van Es et al., 2012) or $DCLK1^+$ IECs (Westphalen et al., 2014), colonic $ATOH1^+$ IECs formed clonal ribbons at a frequency that was at least 10-fold higher under homeostatic conditions. Such a regional difference may simply represent the preferential labeling efficiency of our system or may represent the difference in the population size of $ATOH1^+$ IECs that retain ISC-like properties. Also, as we did not use a multi-color reporter, it remains possible that the $ATOH1^+$ICRs observed *in vivo* may not necessarily represent a single-clone origin but may be composed of multi-cell origin.

These $ATOH1^+$ICRs contained all lineages of differentiated IECs and $Ki\text{-}67^+$ IECs (Figures 3C and 3D), thereby indicating the possibility that the resident $ATOH1^+$ IECs had acquired genuine ISC-specific function and thus took over the whole crypt-villus unit.

Accordingly, analysis of the $ATOH1^+$ICRs in *Lgr5*^{EGFP}*Atoh1*^{tdTomato} mice showed the clear existence of $LGR5\text{-}EGFP^+tdTomato^+$ double-positive IECs in $ATOH1^+$ICRs (Figure 3E). To further verify the acquisition of ISC properties by $ATOH1^+$ IECs, we employed the organoid culture system. Small-intestinal or colonic tissues from *Atoh1*^{tdTomato} mice were subjected to organoid culture at 20 days after RU486 induction. Among the established organoids, we found organoids that completely consisted of $tdTomato^+$ IECs (Figure 3F). These $tdTomato^+$ organoids could be re-organized across passages. The efficiency of forming these $tdTomato^+$ organoids was highly consistent with the time-dependent appearance of $ATOH1^+$ICRs *in vivo* (Figure 3G). Induction of $ATOH1^+$ICR formation appeared to be driven by an IEC-intrinsic mechanism, as

(D) Co-analysis of RNAscope ISH for *Ascl2* (green), with immunostaining for tdTomato (red). *Ascl2*$^+$tdTomato$^+$ double-positive cells are identified in the small-intestinal and colonic crypt. A magnified view of the area identified by the white square is shown in the right side.
(E) qRT-PCR analysis of $CD24^{high}$, $CD24^{mid}$, and $CD24^{low}$ IECs in the small intestine of the wild-type mice (n = 3). Small-intestinal $LGR5^{high}$ IEC population of the *Lgr5*^{EGFP} mice (n = 3) served as a positive control for ISCs. Data are expressed as the mean ± SEM. *p < 0.01.
(F) Representative flow plots of the small-intestinal IECs recovered from the *Atoh1*^{tdTomato} mice on the day following the completion of the five-dose RU486 treatment.
(G and H) qRT-PCR analysis of cell fractions that were acquired in (F).
Data are expressed as the mean ± SEM of values normalized by the expression of β-actin (n = 3 of biological replicates). *p < 0.01, **p < 0.05.
See also Figure S2.

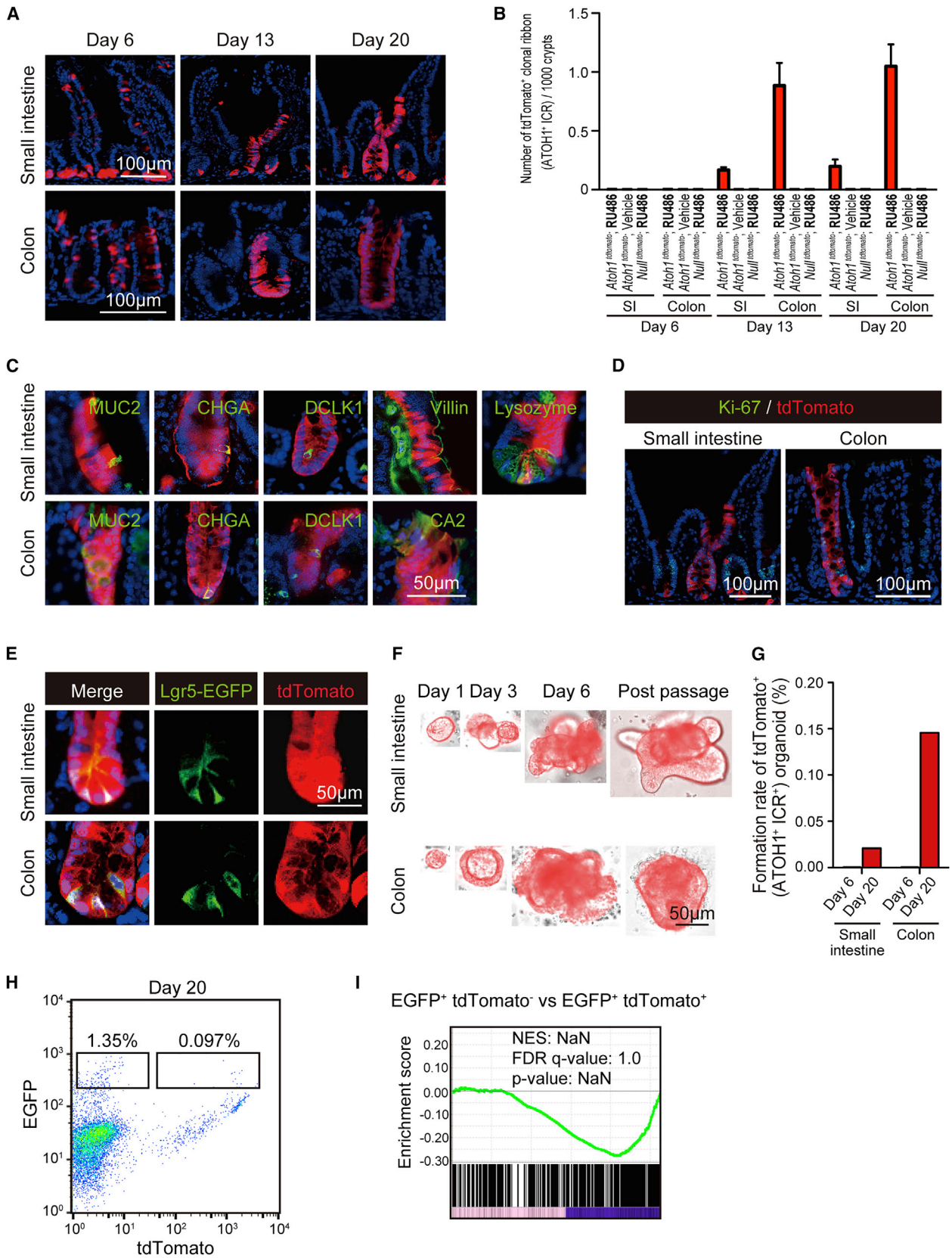

(legend on next page)

tdTomato$^+$ organoids could be formed through RU486-mediated induction *in vitro* (Figure S3A) and maintained beyond passaging (Figure S3B). However, the efficiency of forming tdTomato$^+$ organoids *in vitro* was lower in the organoids of *Atoh1*^{tdTomato} mice than in those of *Lgr5-EGFP-IRES-creERT2; Rosa26-LSL-tdTomato* mice (*Lgr5*^{tdTomato} mice) (Figures S3C and S3D). In addition, tdTomato$^+$ organoids could be re-organized from a single tdTomato$^+$ cell, also at a lower frequency compared with LGR5^{high} cells (Figures S3E and S3F). Those single-cell-derived tdTomato$^+$ organoids could be re-organized beyond passaging (Figure S3G) and give rise to both secretory and absorptive cells (Figure S3H). These results indicate the acquirement of multi-potency by ATOH1$^+$ IECs *in vitro*.

To further identify the properties of ATOH1$^+$ IEC-derived ISCs, LGR5-EGFP$^+$tdTomato$^+$ double-positive ISCs were collected from *Lgr5*^{EGFP}*Atoh1*^{tdTomato} mice on day 20 (Figure 3H), and global gene expression in these cells was compared with LGR5-EGFP$^+$ single-positive ISCs. Gene set enrichment analysis (GSEA) showed that the expression of stem cell-signature genes in LGR5-EGFP$^+$tdTomato$^+$ double-positive ISCs was comparable with that in LGR5-EGFP$^+$ single-positive ISCs (Figure 3I). These results confirmed that a specific population of ATOH1$^+$ IECs is constitutively re-directed to exhibit genuine ISC-specific properties and participate in the maintenance of the normal intestinal epithelium.

Colonic Inflammation Promotes the Generation of ATOH1$^+$ IEC-Derived Clonal Ribbons

Following epithelial injury, various signaling pathways are activated within the intestinal epithelium to aid in optimization of the regeneration program (Okamoto et al., 2009). In the present study, only a minimal increase in the number of small-intestinal ATOH1$^+$ICRs was observed following irradiation-induced damage (control group, 0.20 ribbons per 1,000 crypts; irradiation group, 0.63 ribbons per 1,000 crypts; data not shown). Thus, we examined whether the recruitment of colonic ATOH1$^+$ IECs to the ISC pool and the subsequent formation of ATOH1$^+$ICRs could be enhanced in a dextran sodium sulfate (DSS) colitis model. A significant reduction in body weight in the DSS-colitis mice indicated the successful induction of colitis (Figure S4A). At day 2, we found only a small number of tdTomato$^+$ IECs in the rectum of DSS-colitis mice (Figure S4B). However, at day 6, we found clear increase in the number of tdTomato$^+$ IECs in DSS-colitis mice (Figure 4B). At this time period, LGR5$^+$ATOH1$^+$ double-positive cells were not clearly identified in the rectal crypts of DSS-colitis mice (Figure 4C). However, a clear and persistent existence of ATOH1$^+$ IECs was observed in the rectum of these DSS-colitis mice (Figures S4C and S4D). Accordingly, a significant increase in the mucosal area occupied by tdTomato$^+$ IECs was observed during the recovery phase (day 6, day 13, and day 20) of the damaged mucosa (Figures S4E and S4F). Importantly, ATOH1$^+$ICRs appeared in the rectum of DSS-colitis mice as early as day 6, a time period when they were never observed in the control mice. Some of the massive tdTomato$^+$ area in the DSS-colitis mice at day 13 represented a cluster of tdTomato$^+$ IECs extending from the ulcer-edge crypts, which covered the surface of the adjacent wound (Figure 4D). This observation indicated that ATOH1$^+$ IEC progenies actively contribute to the early phase of tissue repair by forming the wound-associated

Figure 3. ATOH1$^+$ IECs Give Rise to LGR5$^+$ ISCs that Can Form Clonal Ribbons under Homeostatic Conditions

(A) Lineage tracing in *Atoh1*^{tdTomato} mice showing the formation of tdTomato$^+$ clonal ribbons (ATOH1$^+$ICRs) in the small intestine and colon. Mice were treated by the five-dose protocol of RU486 and killed for analysis on day 6, day 13, and day 20.

(B) Quantification of ATOH1$^+$ICR formation frequency in the small intestine and colon, using the tissue sections of *Atoh1*^{tdTomato} mice or mice carrying *Rosa26-LSL-tdTomato* allele alone (*Null*^{tdtomato}). *Atoh1*^{tdTomato} mice treated with vehicle alone (vehicle, n = 3), or *Null*^{tdtomato} mice treated with RU486 (n = 3) served as negative control. Atoh1$^+$ICR was defined as those clusters of tdTomato$^+$ cells completely occupying the whole crypt-villus unit, as assessed by the examination of at least three serial sections. The number of ATOH1$^+$ICR was normalized against the total number of crypts. Data are expressed as the mean ± SEM.

(C) Co-staining of cell-lineage markers, such as MUC2, CHGA, DCLK1, Villin, CA2, and Lysozyme (green) with tdTomato (red) on day 20.

(D) Co-staining of Ki-67 (green) and tdTomato (red) in the Atoh1$^+$ICR observed on day 20.

(E) Fluorescence images of tdTomato$^+$ cells (red) co-expressing Lgr5-EGFP (green) in the ATOH1$^+$ICR of *Lgr5*^{EGFP}*Atoh1*^{tdTomato} mice on day 20. Mice were treated as described in (A).

(F) Successful establishment of tdTomato$^+$ organoids from the small-intestinal and colonic tissues recovered from *Atoh1*^{tdTomato} mice on day 20.

(G) The efficiency of tdTomato$^+$ organoid formation was quantified using tissues collected from the *Atoh1*^{tdTomato} mice. Total cumulative number of tdTomato$^+$ organoids acquired from four mice is normalized by the total number of organoids.

(H) Representative flow plots showing the increased presence of Lgr5-EGFP$^+$tdTomato$^+$ IECs in the small intestine of the *Lgr5*$^{EGFP\text{-}CreERT2}$ *Atoh1*^{tdTomato} mice on day 20 compared with the data on day 6 shown in Figure 2B.

(I) Designated cell fractions in (H) were subjected to microarray analysis and then compared and analyzed for the adult stem cell-specific gene set (M1999) by GSEA.

See also Figure S3.

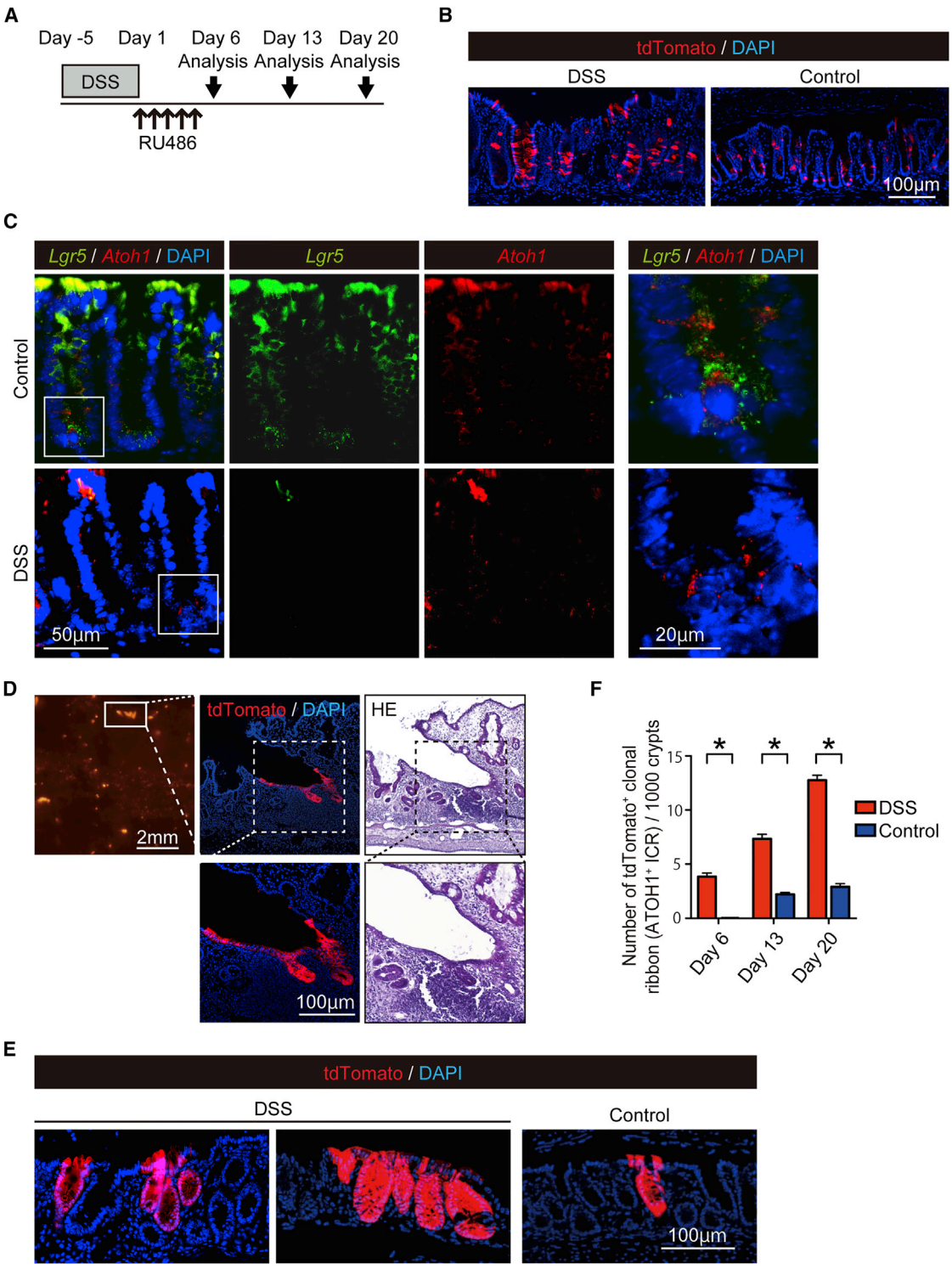

Figure 4. Formation of ATOH1$^+$ IEC-Derived Clonal Ribbon Is Significantly Promoted during Regeneration from Colitis-Induced Epithelial Damage

Formation of ATOH1$^+$ IEC-derived clonal ribbon (ATOH1$^+$ICR) was compared between the DSS-colitis mice (DSS) and control mice (Control).

(A) Experimental design for the lineage-tracing analysis of Atoh1$^+$ IECs in DSS-colitis-induced *Atoh1^{tdTomato}* mice.

(B) Labeling of ATOH1$^+$ IECs-derived cells by tdTomato (red) at day 6 in the colon of DSS-colitis mice and control mice.

(legend continued on next page)

epithelium (Seno et al., 2009). Consequently, we found an increase in the number of ATOH1$^+$ICR formation and massive clusters of ATOH1$^+$ICRs in the rectum of DSS-colitis mice at a later phase (day 20, Figures 4E and 4F). Such an increase in the number of ATOH1$^+$ICR was never found by pre-labeling ATOH1$^+$ cells before DSS treatment (Figures S4G and S4H), thus indicating that colitis-induced ATOH1$^+$ICR formation is initiated by ATOH1$^+$IEC-derived cells that are less sensitive to DSS-induced damage, or ATOH1$^+$ cells that have newly appeared during the post-DSS labeling period.

Collectively, we found that generation of ATOH1$^+$ICRs was significantly promoted at the earliest phase of the tissue repair process in DSS-colitis mice, and thereby partly contributed to the regeneration of colitis-associated wounds.

Inflammatory Cytokines and Bacterial Components Coordinately Promote the Formation of ATOH1$^+$ICRs

To obtain insight into the mechanism underlying the promotion of ATOH1$^+$ICR formation in the colitic environment, the tdTomato$^+$ IEC population in the rectum of DSS-colitis-induced *Atoh1*^{tdTomato} mice was collected (Figure 5A) and subjected to microarray analysis. MA plot analysis identified *Dll1* as one of the highly upregulated genes in the tdTomato$^+$ IEC population of the DSS-colitis mice (Figure 5B). Consistently, a clear increase in the number of DLL1$^+$tdTomato$^+$ double-positive IECs was confirmed in the rectal tissue of the DSS-colitis mice (Figure 5C).

Pathway analysis of the microarray data additionally revealed that gene sets representing the general inflammatory response were most significantly upregulated. Furthermore, we found that the response to interleukin (IL)-1 and TNF-α was significantly upregulated in the ATOH1$^+$ IECs of the DSS-colitis mice (Figure S5A). The NF-κB pathway represents the major downstream signaling pathway shared by TNF-α and IL-1β (Mercurio and Manning, 1999). A previous study highlighted the importance of constitutive NF-κB pathway activation in the de-differentiation of mouse small-intestinal villus IECs (Schwitalla et al., 2013). Our GSEA consistently revealed that the NF-κB pathway gene set was significantly upregulated in the tdTomato$^+$ IECs of the DSS-colitis mice (Figure 5D), as were genes related to stem cell maintenance (Figure 5E). Thus, in DSS colitis, ATOH1$^+$ IEC-derived cells appeared to gain stem cell-like gene expression under an increased activation level of the NF-κB pathway.

To validate the contribution of NF-κB signaling to ATOH1$^+$ICR formation, we performed *in vitro* analyses using organoid culture. Colonic organoids from *Atoh1*^{tdTomato} mice were cultured under DBZ-induced differentiation conditions, which clearly promoted commitment to the ATOH1$^+$ secretory cell lineage, and also promoted downregulation of ISC-specific genes (Figure S5B). To induce activation of the NF-κB pathway, two representative bacterial components, such as lipopolysaccharide (LPS) and flagellin, were employed in addition to TNF-α and IL-1β. The combined addition of these ligands (TILF cocktail) clearly upregulated the expression of IL-8 in DBZ-treated colonic organoids (Figure S5C) and induced the degradation of IκBα (Figure S5D), which confirmed the activation of the NF-κB pathway in secretory cell-committed organoids. Using these secretory cell-committed organoids, we proved that addition of the TILF cocktail could induce the formation of colonic ATOH1$^+$ICRs *in vitro* (Figures 5F and 5G). This *in vitro* formation of ATOH1$^+$ICRs in secretory cell-committed organoids clearly required the addition of all ligands (Figure 5H). Specific blockade of the NF-κB pathway using small-molecule compounds (Figure S5E) consistently inhibited the formation of ATOH1$^+$ICRs in a dose-dependent manner (Figures 5I and S5F). Thus, we found that the NF-κB pathway functions as a key pathway in promoting the exhibition of ISC properties by ATOH1$^+$ IEC-derived cells. Accordingly, the addition of TILF ligands clearly upregulated the expression of ISC markers *Ascl2* and *Smoc2*, in addition to *Dll1* (Figure 5J), suggesting that the expression of these genes may play a key role in the inflammation-induced formation of ATOH1$^+$ICRs. Such a TILF-cocktail-induced upregulation of ISC markers was never observed in organoids treated without DBZ (Figure S5G). However, the expression level of *Lgr5* remained unchanged both in DBZ-treated and untreated organoids (Figures 5I and S5G), possibly due to its low expression level in early reprogrammed ISCs.

To validate the ISC property of TILF-treated Atoh1$^+$IEC-derived cells *in vitro*, we tested whether TILF-treated *Atoh1*^{tdTomoto} mice organoids could newly reconstruct tdTomato$^+$ organoids and expand their progeny beyond passaging. As expected, TILF-treated organoids could reconstruct tdTomato$^+$ organoids beyond passaging from

(C) Double RNAscope ISH showing expression of *Atoh1* (red) and *Lgr5* (green) in the colonic crypts of DSS-colitis mice and control mice. Magnified view of the designated area (white square) is shown in the right end column. Images of the colon are re-used in Figure 2C.
(D) An example of ATOH1$^+$ICR forming the wound-associated epithelium in DSS-colitis mouse on day 13.
(E) Representative rectal sections showing ATOH1$^+$ICRs (red) in the control mice (Control) and in the DSS-colitis mice (DSS) on day 20.
(F) Quantification of the ATOH1$^+$ICR formation frequency in the rectum of DSS-colitis mice (n = 3) and control mice (n = 3). The number of ATOH1$^+$ICR was normalized by the total number of crypts. Data are expressed as the mean ± SEM per 1,000 crypts. *p < 0.0001.
See also Figure S4.

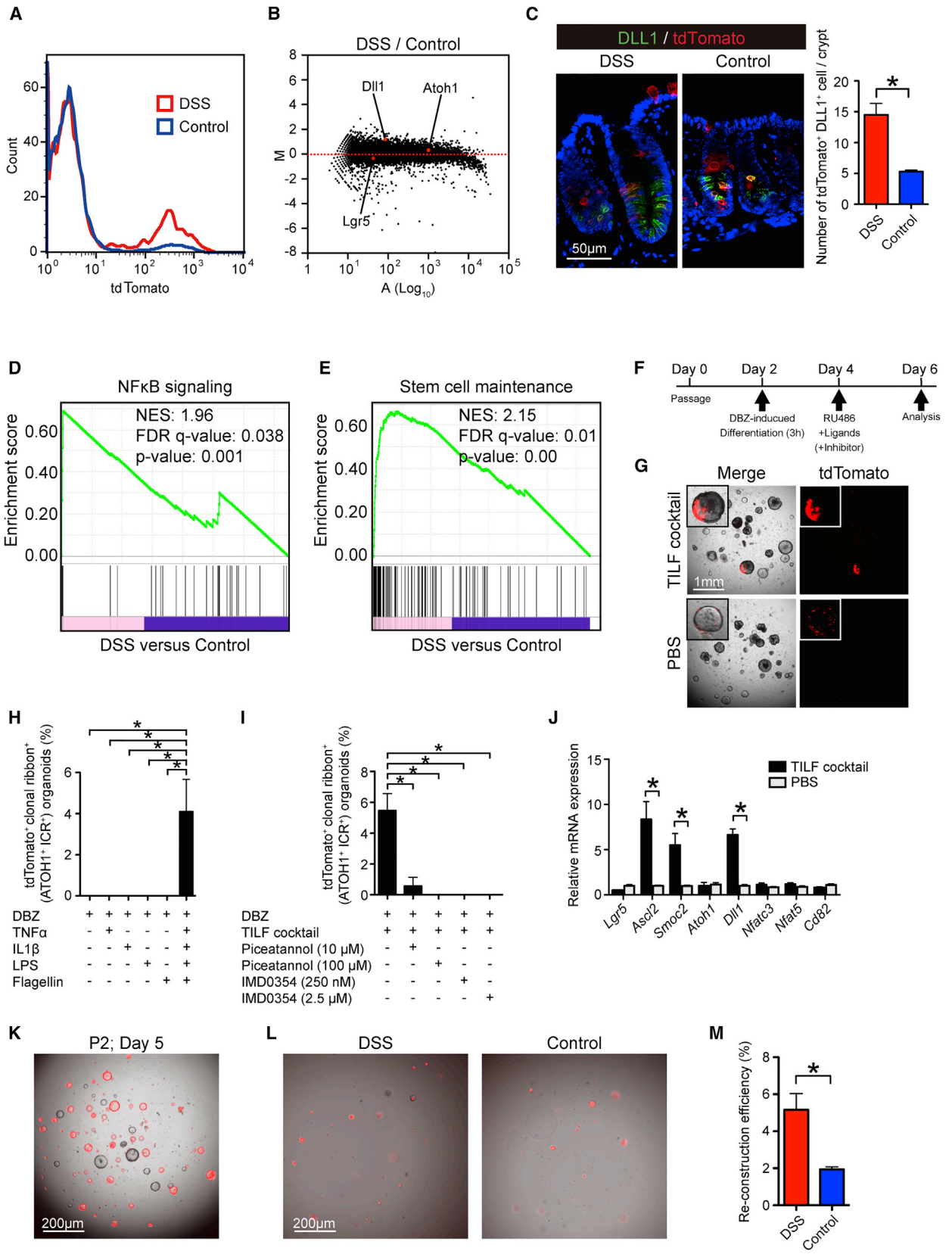

(legend on next page)

single isolated cells (Figure 5K). Also, an increased number of tdTomato$^+$ organoids was re-constructed from single isolated IECs that were recovered from the DSS-colitis mice (Figures 5L and 5M), indicating enrichment of cells retaining ISC-like properties.

ATOH1$^+$ IECs Comprise Colitis-Associated Tumors and Acquire Tumor Stem Cell Properties

CAC develops through a pathway distinct from that of sporadic colon cancer (Feagins et al., 2009; Thorsteinsdottir et al., 2011) and shows pathologic features such as high ATOH1 expression (Kano et al., 2013; Park et al., 2006). However, the precise role of ATOH1$^+$ IECs in CACs remains uncertain. We have previously shown that TNF-α mediated activation of the NF-κB pathway in IECs plays an indispensable role in azoxymethane (AOM)-DSS tumor formation in mice (Onizawa et al., 2009). Hence, we asked whether the tumors of AOM-DSS model mice (Parang et al., 2016) harbor ATOH1$^+$ tumor cells and exhibit features of CACs (Figure 6A). It was found that AOM-DSS tumors contained a substantial number of ATOH1$^+$ tumor cells and expressed ATOH1 at a high level (Figures S6A–S6C). Furthermore, increased production of mucin was observed in these tumors (Figure S6D), suggesting that they faithfully phenocopy CACs.

At the early stage of AOM-DSS tumor labeling in *Atoh1^{tdTomato}* mice, only a few isolated tdTomato$^+$ tumor cells were found (day 56, Figure 6B). However, clear expansion of the tdTomato$^+$ area within the tumor was observed after day 70, which represented a continuous cluster of tdTomato$^+$ tumor cells (Figures 6C and 6D). The ratio of these tumor ATOH1$^+$ICRs among tumor-forming ducts did not increase during the tumor development (Figure 6D), but they clearly included Ki-67$^+$ cells and ATOH1$^+$ cells and showed nuclear translocation of β-catenin (Figure 6E). In contrast, they lacked expression of secretory cell markers other than MUC2 (Figure S6E). Importantly, some of the tdTomato$^+$ cells co-expressed tumor stem cell markers such as CD44 or CD133 (Zeilstra et al., 2008; Zhu et al., 2009) (Figure S6F). Moreover, *Lgr5*$^+$ cells were present in the tdTomato$^+$ tumor clonal ribbons, as shown by the RNAscope ISH analysis (Figure 6F). Consistent with this finding, LGR5-EGFP$^+$tdTomato$^+$ double-positive tumor cells were found in the AOM-DSS tumors of the *Lgr5^{EGFP}Atoh1^{tdTomato}* mice, in addition to LGR5-EGFP$^+$ single-positive tumor cells (Figure 6G). Taken together, these results collectively indicated that ATOH1$^+$ IECs contributed to the development of AOM-DSS tumors by acquiring tumor stem cell properties. However, the existence of LGR5-EGFP$^+$ single-positive tumor cells

Figure 5. Inflammatory Cytokines and Bacterial Components Coordinately Promote the Formation of ATOH1$^+$ICRs

(A) Representative histogram of rectal tdTomato$^+$ IECs in the DSS-colitis mice (red) and control mice (blue) on day 6.

(B) MA plot demonstrating difference in global gene expression between tdTomato$^+$ IECs of DSS-colitis mice and control mice.

(C) Double immunostaining of DLL1 (green) and tdTomato (red) using colonic tissues of DSS-colitis mice and control mice at day 6. The number of tdTomato$^+$DLL1$^+$ double-positive cells was quantified by analysis of rectal tissue obtained from DSS-colitis mice (n = 3) and control mice (n = 3). Data are expressed as the mean ± SEM. *p < 0.05.

(D) The global gene expression data from (B) were compared with the registered NF-κB signaling gene set (M1983) through GSEA.

(E) The global gene expression data from (B) were compared with the registered adult stem cell gene set (M1999) through GSEA.

(F) *In vitro* analysis of ATOH1$^+$ICR formation using colonic organoids from *Atoh1^{tdTomato}* mice. Organoids were cultured under DBZ-induced secretory lineage-differentiation conditions for 3 hr and subjected to *in vitro* lineage-tracing analysis following the addition of RU486 with cytokines or bacterial components (Ligands). The addition of PBS alone served as a control.

(G) Phase-contrast view and tdTomato fluorescence view (red) of the organoids treated as shown in (F). The data are from organoids on day 6. Note that the organoids in the control condition (PBS) showed a scattered distribution pattern of tdTomato$^+$ IECs, whereas those treated with the combination of TNF-α, IL-1β, LPS, and flagellin (TILF cocktail) clearly showed a continuous stream of tdTomato$^+$ IECs (upper left inset).

(H) Quantitative analysis of the *in vitro* lineage-tracing analysis. The number of organoids showing *in vitro* ATOH1$^+$ICR was normalized by the total organoids that were established during the experimental period. The presented data are from three independent analyses including over 100 organoids from each experimental condition. Data are expressed as the mean ± SEM. *p < 0.05.

(I) Quantitative analysis of the *in vitro* lineage-tracing analysis. Data are expressed as the mean ± SEM (three independent analyses). *p < 0.05. Piceatannol or IMD0354 was added at the same time as the TILF cocktail.

(J) qPCR analysis of colonic organoids. Data are expressed as the mean ± SEM of values normalized against the expression of β-actin (three independent analyses). *p < 0.05.

(K) Single-cell organoid reconstruction assay of colonic organoids treated by TILF cocktail. Colonic organoids were treated as described in (F), and those TILF-treated tdTomato$^+$ organoids were further subjected to single-cell passage. Picture shows organoids at day 5 after second passage from TILF addition (P2; Day5).

(L) Single-cell organoid reconstruction assay using colonic IECs isolated from DSS-colitis mice or control mice at day 3.

(M) Quantification of organoid reconstruction assay shown in (L), using DSS-colitis mice (n = 3) and control mice (n = 3). Data are expressed as the mean ± SEM. *p < 0.001.

See also Figure S5.

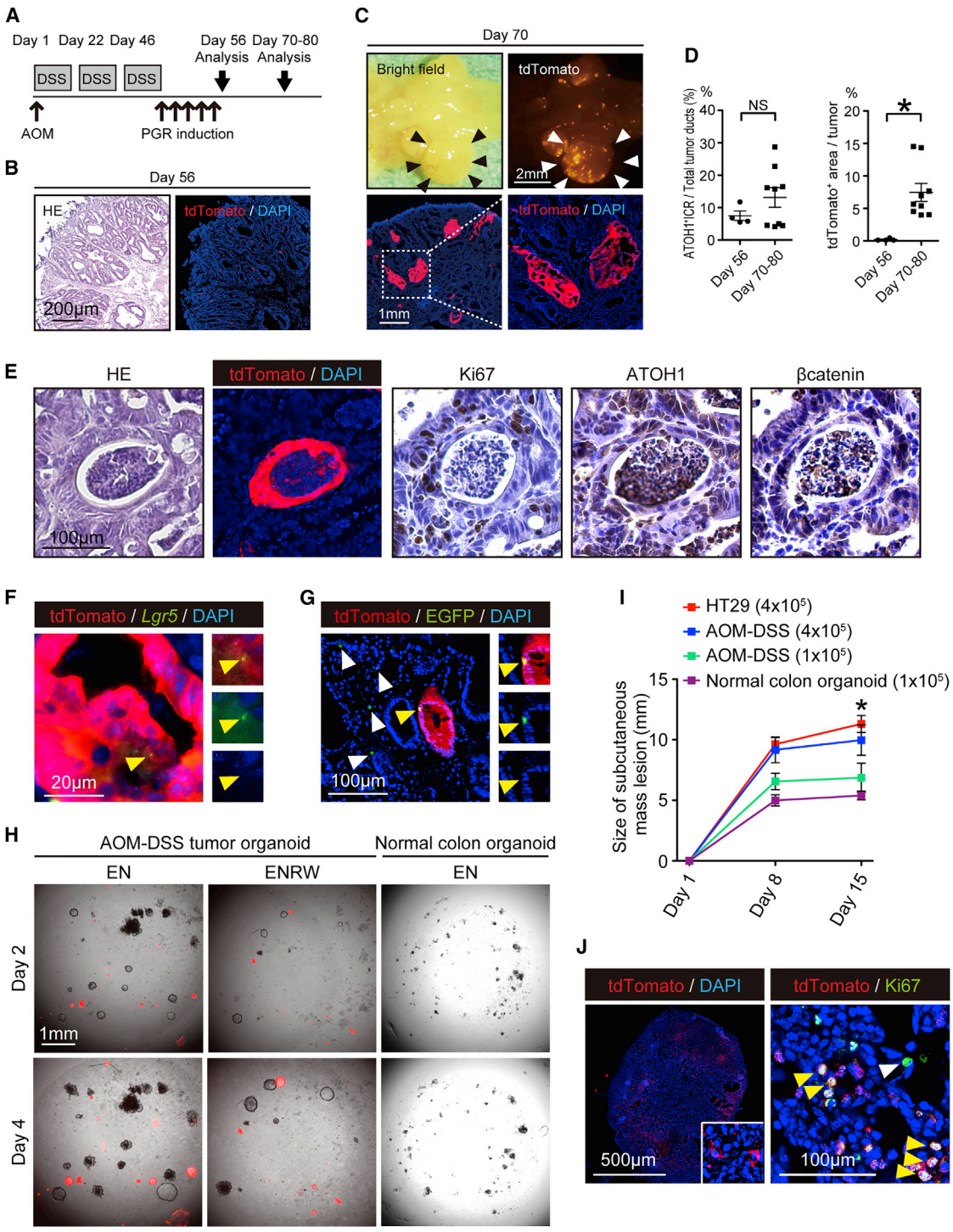

Figure 6. ATOH1$^+$ IECs Contribute to the Formation of AOM-DSS-Induced Colitic Tumors and Acquire the Properties of Tumor Stem Cells

(A) Experimental design combining the AOM-DSS tumor model and ATOH1$^+$ IEC lineage tracing.

(B) H&E staining and fluorescence images of a rectal tumor tissue section on day 56. A few isolated tdTomato$^+$ cells (red) were found within the tumor tissue.

(C) Stereoscopic view (upper panels) and tissue section (lower panels) of a massive rectal tumor (black and white arrowheads) on day 70.

(legend continued on next page)

indicated that these AOM-DSS tumors were mosaic and potentially consisted of a heterogeneous population of ATOH1$^+$ and ATOH1$^-$ tumor stem cells.

As expected, we observed that both tdTomato$^+$ and tdTomato$^-$ AOM-DSS tumor cell organoids could be established *in vitro* (Figure 6H). The tdTomato$^+$ AOM-DSS tumor organoids consisted solely of tdTomato$^+$ cells and shared the Wnt-independent growth ability of the tdTomato$^-$ tumor organoids. Furthermore, they could be maintained across several passages and form tumors via subcutaneous transplantation into nude mice in a dose-dependent manner (Figure 6I). The re-produced tumors of the nude mice consisted of both tdTomato$^+$ and tdTomato$^-$ proliferating cells (Figure 6J), which conserved the mosaic features of the original AOM-DSS tumor. These results collectively indicated that AOM-DSS tumors harbored ATOH1$^+$ IEC-derived tumor stem cells, in addition to tumor stem cells of other origins. Thus, colitis-associated tumorigenesis may represent another pathologic condition in which the acquisition of stem cell-like properties by ATOH1$^+$ IECs can be promoted.

DISCUSSION

In our lineage-tracing model, the frequency of forming colonic ATOH1$^+$ICRs reached 250–300 ribbons per mouse under homeostatic conditions and 1,500–1,800 ribbons per mouse in DSS colitis, which certainly exceeded previous models (Tetteh et al., 2016; van Es et al., 2012; Westphalen et al., 2014). Thus, our results highlight the contribution of ATOH1$^+$ IECs in the maintenance of the ISC pool, particularly in the colon. We also succeeded in clearly visualizing the dramatic and time-dependent increase in the frequency of colonic ATOH1$^+$ICR formation in the DSS-colitis model. This result underpins the previous report of DCLK1$^+$ IECs, which indicated the increased ISC conversion of colonic DCLK1$^+$ IECs in DSS-colitis mice but did not successfully identify increased formation of DCLK1$^+$ IEC-derived clonal ribbons (Westphalen et al., 2014).

Previous studies have identified at least three subpopulations of small-intestinal ATOH1$^+$ IECs that may retain their potential to undergo conversion back to ISCs: ATOH1$^+$LGR5$^+$ double-positive IECs at the +1 to +3 position (Kim et al., 2016), ATOH1$^+$LRCs at the +4 position (Buczacki et al., 2013), and ATOH1$^+$DLL1$^+$ IECs at the +5 position (van Es et al., 2012). However, the origin of cells that can form colonic ATOH1$^+$ICRs may be heterogeneous and may differ from the small-intestinal counterparts. For example, the existence of colonic LRCs is not well confirmed, and small-intestinal LRCs have never been shown to form clonal ribbons under homeostatic conditions (Kim et al., 2016). The existence of ATOH1$^+$LGR5$^+$ double-positive IECs in the normal or colitic colon has never been identified in previous reports. In our current analysis, we successfully identified a rare population of ATOH1$^+$LGR5$^+$ double-positive cells both in the small intestine and colon (Figure 2C). However, most of these ATOH1$^+$LGR5$^+$ double-positive cells appeared to be lost under induction of DSS colitis (Figure 4C). Therefore, ATOH1$^+$LGR5$^+$ double-positive cells may be the dominant origin of ATOH1$^+$ICRs under homeostatic conditions but may be less involved in ATOH1$^+$ICR formation under DSS colitis.

We have previously shown that DLL1$^+$ IECs reside at the lowest part of the crypts, both in the small intestine and in

(D) Percentage ratio of tumor ATOH1$^+$ICR or the area occupied by tdTomato$^+$ tumor cells was analyzed in tumors at day 56 (n = 4) and day 70–80 (n = 8). Data are expressed as the mean ± SEM. *p < 0.05, N.S., not significant.
(E) Staining of serial sections showing ATOH1$^+$, Ki-67$^+$, and nuclear-localized β-catenin$^+$ cells in the tumor ATOH1$^+$ICR on day 70.
(F) RNAscope ISH analysis showing a *Lgr5*$^+$ (green) tumor cell (yellow arrowhead) within the tdTomato$^+$ (red) tumor area.
(G) *Lgr5*^{EGFP}*Atoh1*^{tdTomato} mice were treated as shown in (A). Lgr5-EGFP$^+$ tdTomato$^+$ double-positive tumor cells (yellow arrowhead) were found within the tumor ATOH1$^+$ICRs of the rectal tumors on day 69, along with Lgr5-EGFP$^+$ single-positive tumor cells in the surrounding tumor area (white arrowhead).
(H) Organoid culture using AOM-DSS tumor tissues from *Atoh1*^{tdTomato} mice or normal colonic tissues from wild-type mice. Isolated cells were cultured in Wnt3a/R-Spondin-1-supplemented medium (ENRW) or Wnt3a/R-Spondin-1-depleted medium (EN). A merged view of the phase-contrast and tdTomato fluorescence (red) images is shown.
(I) Growth of subcutaneous tumors initiated by transplantation of AOM-DSS tumor-cell-derived organoids (1×10^5 cells, n = 3; 4×10^5 cells, n = 3; AOM-DSS), normal colon-derived organoids (1×10^5 cells, n = 3; normal colon organoid), or HT29 cells (4×10^5 cells, n = 3; HT29) into nude mice. For the transplantation of AOM-DSS tumor cell-derived organoids, a mixture of tdTomato$^+$ and tdTomato$^-$ organoids was used. Data are expressed as the mean ± SEM. * indicates p < 0.001 of HT-29 and AOM-DSS (4×10^5) compared with normal colon organoid.
(J) Tissue analysis of the tumors formed through transplantation of AOM-DSS tumor cell-derived organoids (4×10^5 cells). Macroscopic view (left panel) showing the distribution of tdTomato$^+$ cells (red) in a mosaic pattern. Immunostaining for tdTomato (red) and Ki67 (green) revealing a cluster of Ki67$^+$tdTomato$^+$ double-positive cells (yellow arrowhead) within the tumor tissue. In addition, Ki67$^+$tdTomato$^-$ single-positive cells were found within the surrounding tumor tissue (white arrowhead).
See also Figure S6.

the colon (Shimizu et al., 2014). Furthermore, an increase of DLL1$^+$ colonic IECs was clearly confirmed in DSS-colitis mice (Figure 5C) (Shimizu et al., 2014). Therefore, the DLL1$^+$ population of ATOH1$^+$ IEC-derived cells may be one of the candidate subpopulations that can form ATOH1$^+$ICRs in the colon, especially under inflammatory conditions. However, it remains possible that the increase of ATOH1$^+$ICR formation in DSS-colitis mice depends on the concerted contribution of other unknown subpopulations. A similar de-differentiation has been observed in the airway secretory lineage IECs, suggesting that re-acquiring stem cell properties is inversely related to their maturity (Tata et al., 2013).

Our analysis of ATOH1$^+$ IECs in DSS-colitis mice successfully identified cytokine- or bacterial-component-induced NF-κB activation as a key event in promoting ATOH1$^+$ICR formation (Figures 5D–5J), which is consistent with a previous study involving genetic NF-κB activation in villus IECs (Schwitalla et al., 2013). Because NF-κB pathway activation in secretory lineage-committed organoids appeared to upregulate the expression of *Dll1* (Figure 5J), it may be possible that NF-κB signaling promotes ATOH1$^+$ICR formation via generating an increased number of DLL1$^+$ secretory progenitor cells.

In the AOM-DSS model, ATOH1$^+$ IECs acquired the properties of tumor stem cells and appeared to contribute to the mosaic development of tumors (Figure 6C). At present, it remains uncertain to what extent these cells precisely contribute to the overall development and progression of these tumors. The contribution of ATOH1$^+$ tumor cells to the overall tumor formation may be underestimated due to the limited labeling efficiency of the present lineage-tracing system. However, the clear mosaic pattern harboring both ATOH1$^+$ and ATOH1$^-$ tumor stem cells may illustrate one of the reasons why colitis-associated tumors are highly resistant to chemotherapeutic approaches. Recently, it has been shown that human colorectal cancer cells can interconvert between differentiated tumor cells and tumor stem cells, thereby exhibiting resistance to tumor stem cell-specific ablation (Shimokawa et al., 2017). Further studies will be needed to confirm the contribution of ATOH1$^+$ tumor cells to the heterogeneous development and progression of CACs found in IBD patients. Nevertheless, our results newly indicate ATOH1$^+$ tumor cells as an additional therapeutic target cell population for CACs.

EXPERIMENTAL PROCEDURES

Mice

C57BL/6J mice and BALB/cAJcl-*nu*/*nu* mice were purchased from Japan Clea.

Atoh1$^{Cre\text{-}PGR}$ (Rose et al., 2009), *Lgr5-EGFP-IRES-creERT2* (Barker et al., 2007), *Rosa26-LSL-tdTomato* mice (Madisen et al., 2010), or *Apc*^{Min} mice were purchased from the Jackson Laboratory. *Apc*$^{fl/fl}$ mice were provided by RIKEN BRC (Colnot et al., 2004). The primers used for genotyping are listed in Table S1. Male and female mice at 8–10 weeks of age were used. All animal experiments were approved by the Animal Care and Use Committee of Tokyo Medical and Dental University (0160326A and 0170276A). For the induction of Cre-mediated recombination, mifepristone (RU486, 2 mg/body, Sigma-Aldrich) or tamoxifen (TMX, 2 mg/body, Sigma-Aldrich) was injected intraperitoneally into mice carrying the *Atoh1*$^{Cre\text{-}PGR}$ allele or the *Lgr5-EGFP-IRES-creERT2* allele, respectively.

Immunohistochemistry

Immunohistochemistry was performed as previously described (Okamoto et al., 2009). The primary antibodies employed for these assays are listed in Table S2. Antigen retrieval using citrate buffer was required for the staining of ATOH1, HES1 (Ito et al., 2000), chromogranin A (CHGA), DCLK1, Ki-67, tdTomato, and β-CATENIN.

ACCESSION NUMBERS

Microarray data have been deposited in the Gene Expression Omnibus under accession numbers GEO: GSE81315 and GSE81451.

SUPPLEMENTAL INFORMATION

Supplemental Information includes Supplemental Experimental Procedures, six figures, and three tables and can be found with this article online at https://doi.org/10.1016/j.stemcr.2017.11.006.

AUTHOR CONTRIBUTIONS

F.I., H.S., R.K., T. Nakata, and G.I. performed the histology experiments. F.I., S.F., S.A., K.S., and A.K. performed the organoid culture experiments under the supervision of T. Murano and T. Mizutani. Mouse experiments were performed by F.I. and S.N. under the supervision of S.O. and K.T. T. Nakamura and M.W. supervised the entire project. F.I. and R.O. wrote the manuscript.

ACKNOWLEDGMENTS

We thank Dr. Tetsuo Sudo (Toray Industry) and Prof. Jane E. Johnson (UT Southwestern) for providing antibodies. This work was supported by MEXT/JSPS KAKENHI (16H05284, 226221307) and the Research Center Network Program and Practical Research Project from AMED (16bm0304001h0004, 17bm0304001h0005, 17ek0109188h0002).

Received: May 18, 2017
Revised: November 4, 2017
Accepted: November 5, 2017
Published: December 7, 2017

REFERENCES

Barker, N., van Es, J.H., Kuipers, J., Kujala, P., van den Born, M., Cozijnsen, M., Haegebarth, A., Korving, J., Begthel, H., Peters, P.J., and Clevers, H. (2007). Identification of stem cells in small intestine and colon by marker gene Lgr5. Nature *449*, 1003–1007.

Barker, N., Ridgway, R.A., van Es, J.H., van de Wetering, M., Begthel, H., van den Born, M., Danenberg, E., Clarke, A.R., Sansom, O.J., and Clevers, H. (2009). Crypt stem cells as the cells-of-origin of intestinal cancer. Nature *457*, 608–611.

Buczacki, S.J.A., Zecchini, H.I., Nicholson, A.M., Russell, R., Vermeulen, L., Kemp, R., and Winton, D.J. (2013). Intestinal label-retaining cells are secretory precursors expressing Lgr5. Nature *495*, 65–69.

Colnot, S., Niwa-Kawakita, M., Hamard, G., Godard, C., Le Plenier, S., Houbron, C., Romagnolo, B., Berrebi, D., Giovannini, M., and Perret, C. (2004). Colorectal cancers in a new mouse model of familial adenomatous polyposis: influence of genetic and environmental modifiers. Lab. Invest. *84*, 1619–1630.

Davis, H., Irshad, S., Bansal, M., Rafferty, H., Boitsova, T., Bardella, C., Jaeger, E., Lewis, A., Freeman-Mills, L., Giner, F.C., et al. (2015). Aberrant epithelial GREM1 expression initiates colonic tumorigenesis from cells outside the stem cell niche. Nat. Med. *21*, 62–70.

Feagins, L.A., Souza, R.F., and Spechler, S.J. (2009). Carcinogenesis in IBD: potential targets for the prevention of colorectal cancer. Nat. Rev. Gastroenterol. Hepatol. *6*, 297–305.

Fukushima, K., Tsuchiya, K., Kano, Y., Horita, N., Hibiya, S., Hayashi, R., Kitagaki, K., Negi, M., Itoh, E., Akashi, T., et al. (2015). Atonal homolog 1 protein stabilized by tumor necrosis factor α induces high malignant potential in colon cancer cell line. Cancer Sci. *106*, 1000–1007.

Ito, T., Udaka, N., Yazawa, T., Okudela, K., Hayashi, H., Sudo, T., Guillemot, F., Kageyama, R., and Kitamura, H. (2000). Basic helix-loop-helix transcription factors regulate the neuroendocrine differentiation of fetal mouse pulmonary epithelium. Development *127*, 3913–3921.

Jensen, J., Pedersen, E.E., Galante, P., Hald, J., Heller, R.S., Ishibashi, M., Kageyama, R., Guillemot, F., Serup, P., and Madsen, O.D. (2000). Control of endodermal endocrine development by Hes-1. Nat. Genet. *24*, 36–44.

Kano, Y., Tsuchiya, K., Zheng, X., Horita, N., Fukushima, K., Hibiya, S., Yamauchi, Y., Nishimura, T., Hinohara, K., Gotoh, N., et al. (2013). The acquisition of malignant potential in colon cancer is regulated by the stabilization of Atonal homolog 1 protein. Biochem. Biophys. Res. Commun. *432*, 175–181.

Kim, T.-H., Saadatpour, A., Guo, G., Saxena, M., Cavazza, A., Desai, N., Jadhav, U., Jiang, L., Rivera, M.N., Orkin, S.H., et al. (2016). Single-cell transcript profiles reveal multilineage priming in early progenitors derived from Lgr5(+) intestinal stem cells. Cell Rep. *16*, 2053–2060.

Madisen, L., Zwingman, T.A., Sunkin, S.M., Oh, S.W., Zariwala, H.A., Gu, H., Ng, L.L., Palmiter, R.D., Hawrylycz, M.J., Jones, A.R., et al. (2010). A robust and high-throughput Cre reporting and characterization system for the whole mouse brain. Nat. Neurosci. *13*, 133–140.

Mercurio, F., and Manning, A.M. (1999). Multiple signals converging on NF-kappaB. Curr. Opin. Cell Biol. *11*, 226–232.

Mills, J.C., and Sansom, O.J. (2015). Reserve stem cells: differentiated cells reprogram to fuel repair, metaplasia, and neoplasia in the adult gastrointestinal tract. Sci. Signal. *8*, re8.

Okamoto, R., and Watanabe, M. (2016). Role of epithelial cells in the pathogenesis and treatment of inflammatory bowel disease. J. Gastroenterol. *51*, 11–21.

Okamoto, R., Tsuchiya, K., Nemoto, Y., Akiyama, J., Nakamura, T., Kanai, T., and Watanabe, M. (2009). Requirement of Notch activation during regeneration of the intestinal epithelia. Am. J. Physiol. Gastrointest. Liver Physiol. *296*, G23–G35.

Onizawa, M., Nagaishi, T., Kanai, T., Nagano, K.-I., Oshima, S., Nemoto, Y., Yoshioka, A., Totsuka, T., Okamoto, R., Nakamura, T., et al. (2009). Signaling pathway via TNF-alpha/NF-kappaB in intestinal epithelial cells may be directly involved in colitis-associated carcinogenesis. Am. J. Physiol. Gastrointest. Liver Physiol. *296*, G850–G859.

Parang, B., Barrett, C.W., and Williams, C.S. (2016). AOM/DSS model of colitis-associated cancer. Methods Mol. Biol. *1422*, 297–307.

Park, E.T., Oh, H.K., Gum, J.R., Crawley, S.C., Kakar, S., Engel, J., Leow, C.C., Gao, W.Q., and Kim, Y.S. (2006). HATH1 expression in mucinous cancers of the colorectum and related lesions. Clin. Cancer Res. *12*, 5403–5410.

Rose, M.F., Ahmad, K.A., Thaller, C., and Zoghbi, H.Y. (2009). Excitatory neurons of the proprioceptive, interoceptive, and arousal hindbrain networks share a developmental requirement for Math1. Proc. Natl. Acad. Sci. USA *106*, 22462–22467.

Sato, T., van Es, J.H., Snippert, H.J., Stange, D.E., Vries, R.G., van den Born, M., Barker, N., Shroyer, N.F., van de Wetering, M., and Clevers, H. (2012). Paneth cells constitute the niche for Lgr5 stem cells in intestinal crypts. Nature *469*, 415–418.

Schonhoff, S.E., Giel-Moloney, M., and Leiter, A.B. (2004). Neurogenin 3-expressing progenitor cells in the gastrointestinal tract differentiate into both endocrine and non-endocrine cell types. Dev. Biol. *270*, 443–454.

Schwitalla, S., Fingerle, A.A., Cammareri, P., Nebelsiek, T., Göktuna, S.I., Ziegler, P.K., Canli, O., Heijmans, J., Huels, D.J., Moreaux, G., et al. (2013). Intestinal tumorigenesis initiated by dedifferentiation and acquisition of stem-cell-like properties. Cell *152*, 25–38.

Seno, H., Miyoshi, H., Brown, S.L., Geske, M.J., Colonna, M., and Stappenbeck, T.S. (2009). Efficient colonic mucosal wound repair requires Trem2 signaling. Proc. Natl. Acad. Sci. USA *106*, 256–261.

Shimizu, H., Okamoto, R., Ito, G., Fujii, S., Nakata, T., Suzuki, K., Murano, T., Mizutani, T., Tsuchiya, K., Nakamura, T., et al. (2014). Distinct expression patterns of Notch ligands, Dll1 and Dll4, in normal and inflamed mice intestine. PeerJ *2*, e370.

Shimokawa, M., Ohta, Y., Nishikori, S., Matano, M., Takano, A., Fujii, M., Date, S., Sugimoto, S., Kanai, T., and Sato, T. (2017). Visualization and targeting of LGR5(+) human colon cancer stem cells. Nature *545*, 187–192.

Tata, P.R., Mou, H., Pardo-Saganta, A., Zhao, R., Prabhu, M., Law, B.M., Vinarsky, V., Cho, J.L., Breton, S., Sahay, A., et al. (2013). Dedifferentiation of committed epithelial cells into stem cells in vivo. Nature *503*, 218–223.

Tetteh, P.W., Basak, O., Farin, H.F., Wiebrands, K., Kretzschmar, K., Begthel, H., van den Born, M., Korving, J., de Sauvage, F., van Es, J.H., et al. (2016). Replacement of Lost Lgr5-positive stem cells

through plasticity of their enterocyte-lineage daughters. Cell Stem Cell *18*, 203–213.

Thorsteinsdottir, S., Gudjonsson, T., Nielsen, O.H., Vainer, B., and Seidelin, J.B. (2011). Pathogenesis and biomarkers of carcinogenesis in ulcerative colitis. Nat. Rev. Gastroenterol. Hepatol. *8*, 395–404.

van Es, J.H., Sato, T., van de Wetering, M., Lyubimova, A., Nee, A.N.Y., Gregorieff, A., Sasaki, N., Zeinstra, L., van den Born, M., Korving, J., et al. (2012). Dll1+ secretory progenitor cells revert to stem cells upon crypt damage. Nat. Cell Biol. *14*, 1099–1104.

von Furstenberg, R.J., Gulati, A.S., Baxi, A., Doherty, J.M., Stappenbeck, T.S., Gracz, A.D., Magness, S.T., and Henning, S.J. (2011). Sorting mouse jejunal epithelial cells with CD24 yields a population with characteristics of intestinal stem cells. Am. J. Physiol. Gastrointest. Liver Physiol. *300*, G409–G417.

Westphalen, C.B., Asfaha, S., Hayakawa, Y., Takemoto, Y., Lukin, D.J., Nuber, A.H., Brandtner, A., Setlik, W., Remotti, H., Muley, A., et al. (2014). Long-lived intestinal tuft cells serve as colon cancer-initiating cells. J. Clin. Invest. *124*, 1283–1295.

Yang, Q., Bermingham, N.A., Finegold, M.J., and Zoghbi, H.Y. (2001). Requirement of Math1 for secretory cell lineage commitment in the mouse intestine. Science *294*, 2155–2158.

Zeilstra, J., Joosten, S.P.J., Dokter, M., Verwiel, E., Spaargaren, M., and Pals, S.T. (2008). Deletion of the WNT target and cancer stem cell marker CD44 in Apc(Min/+) mice attenuates intestinal tumorigenesis. Cancer Res. *68*, 3655–3661.

Zhu, L., Gibson, P., Currle, D.S., Tong, Y., Richardson, R.J., Bayazitov, I.T., Poppleton, H., Zakharenko, S., Ellison, D.W., and Gilbertson, R.J. (2009). Prominin 1 marks intestinal stem cells that are susceptible to neoplastic transformation. Nature *457*, 603–607.

Stem Cell Reports, Volume *10*

Supplemental Information

Contribution of ATOH1^{+} Cells to the Homeostasis, Repair, and Tumorigenesis of the Colonic Epithelium

Fumiaki Ishibashi, Hiromichi Shimizu, Toru Nakata, Satoru Fujii, Kohei Suzuki, Ami Kawamoto, Sho Anzai, Reiko Kuno, Sayaka Nagata, Go Ito, Tatsuro Murano, Tomohiro Mizutani, Shigeru Oshima, Kiichiro Tsuchiya, Tetsuya Nakamura, Mamoru Watanabe, and Ryuichi Okamoto

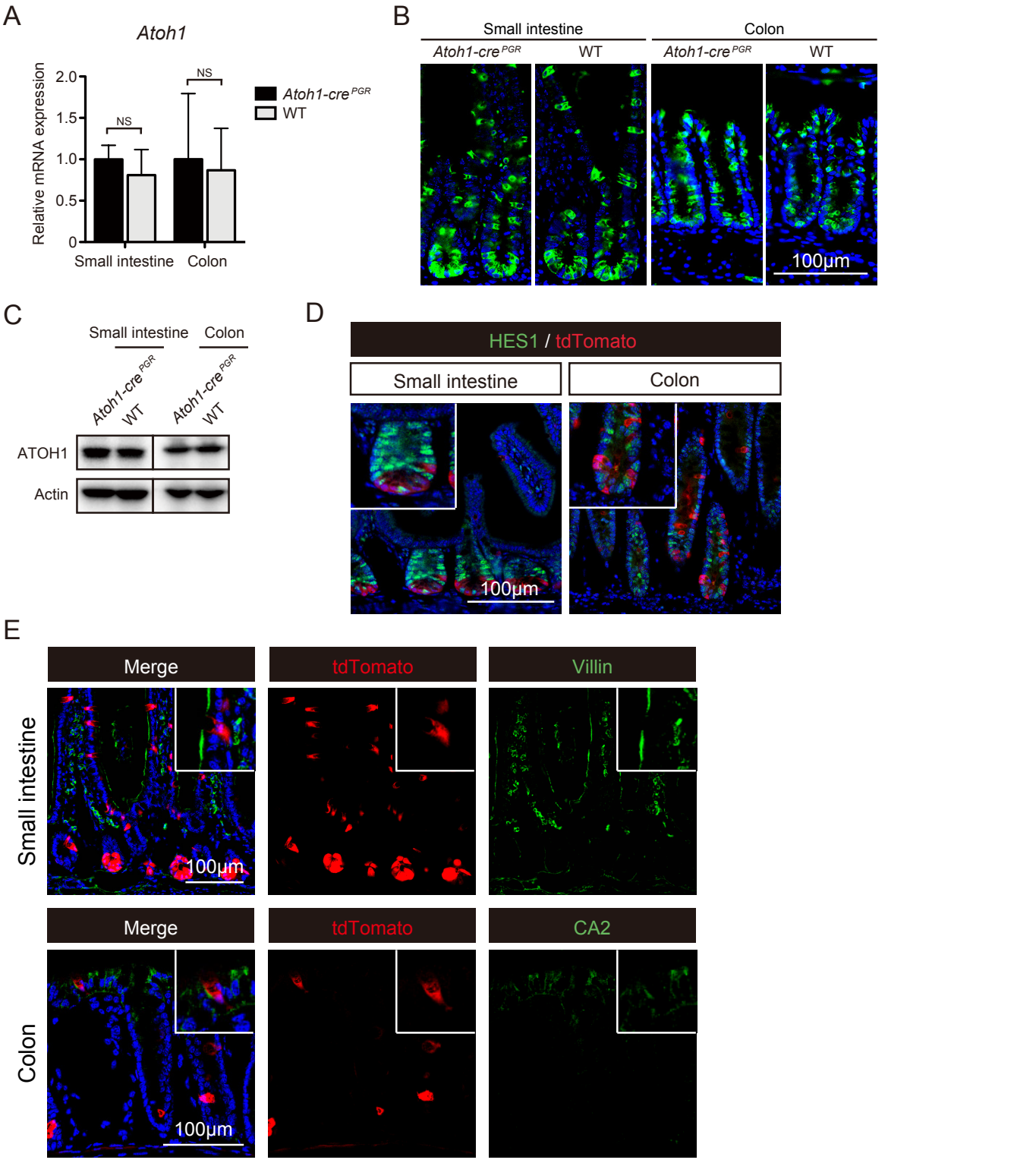

Figure S1. Related to Figure 1. Analysis of *Atoh1*^{tdTomato} mice under homeostatic condition.
(A) Quantitative RT-PCR analysis of *Atoh1* mRNA expression in wild-type mice (WT, n=3) and mice carrying the *Atoh1crePGR* knock-in allele (*Atoh1-crePGR*, n=3). Data are expressed as the mean±SEM. NS, not significant. (B) Small intestinal and colonic tissues of wild-type mice (WT) and mice carrying the *Atoh-crePGR* knock-in allele (*Atoh1-cre*^{PGR}) were subjected to immunostaining of ATOH1 (green). (C) Immunoblot analysis of ATOH1 expression in the intestinal tissues of wild-type mice (WT) and mice carrying the *Atoh-crePGR* knock-in allele (*Atoh1-cre*^{PGR}). (D) Tissues of *Atoh1*^{tdTomato} mice were collected on the day following the completion of single-dose RU486 induction. Double immunostaining of HES1 (green) and tdTomato (red) revealed their distinct expression patterns, with no double-positive cells being found in the small intestine or colon. A magnified view of the crypt area is shown in the left upper panel. (E) Small intestinal or colonic tissues prepared under the same conditions as in (D) were subjected to double immunostaining of absorptive cell markers and tdTomato. The magnified view in the right upper corner clearly shows that Villin^{+} IECs (green) of the small intestine are not labelled by tdTomato (red) and that CA2^{+} IECs (green) of the colon are not labelled by tdTomato (red).

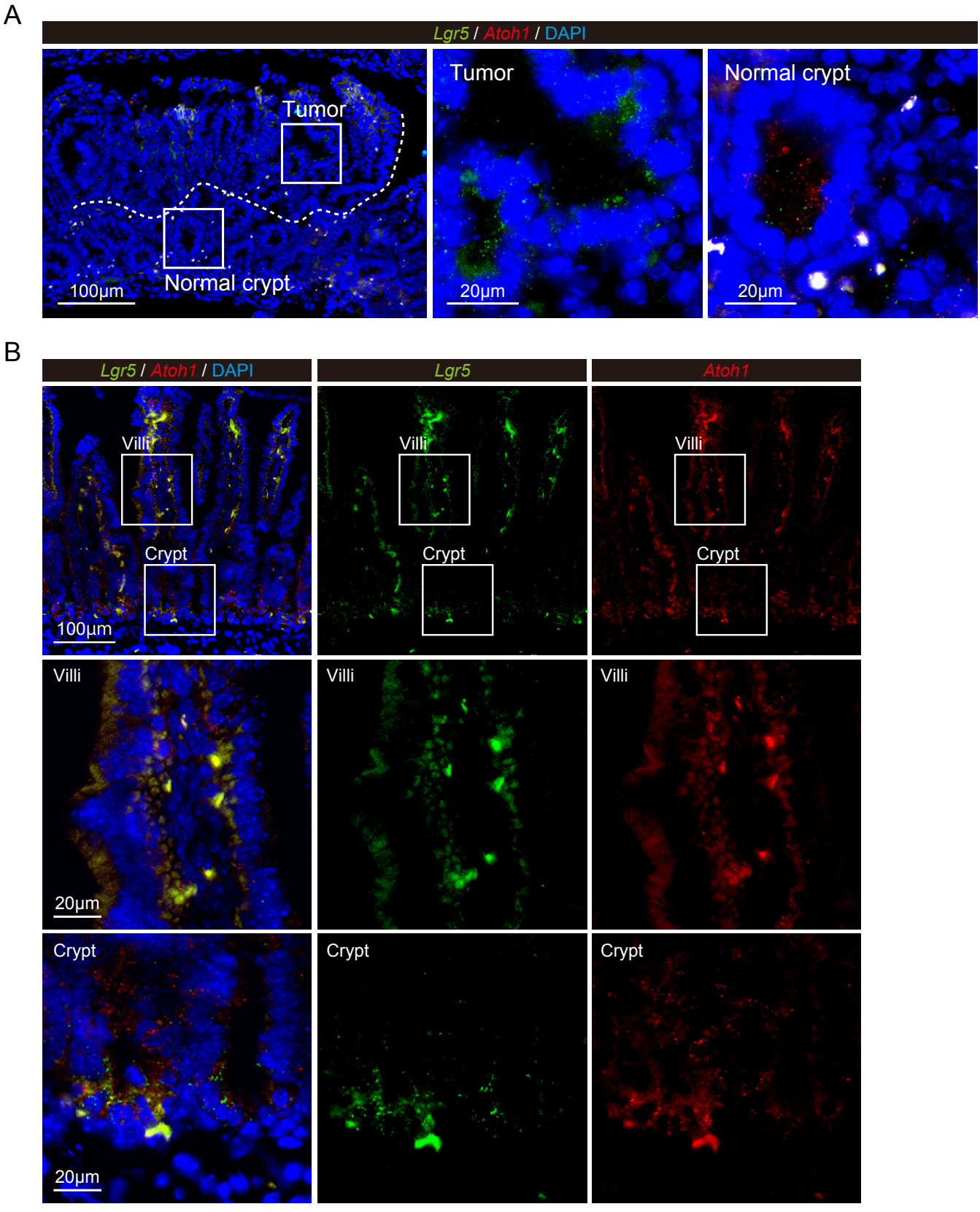

Figure S2. Related to Figure 2. Validation of *Lgr5* and *Atoh1* mRNA detection by RNAscope.
(A) RNAscope analysis of *Lgr5* and *Atoh1* in a small intestinal tumor of an Apc ^{Min} mouse. Robust and abundant signal of *Lgr5* (green) is observed in the tumor region (Tumor). In contrast, *Atoh1* signal is absent in the corresponding region. Signal of both *Lgr5* and *Atoh1* (red) is found in the adjacent non-tumor region (Normal crypt). (A) RNAscope analysis of *Lgr5* and *Atoh1* in a small intestinal tissue of a wild-type mouse. The signal of *Lgr5* (green) is confined to the lower crypt region. In contrast, the signal of *Atoh1* (red) is observed in the lower-to-upper region of the crypt, and also in the villi. Middle column shows magnified images of the villi. Lower column shows magnified images of crypts.

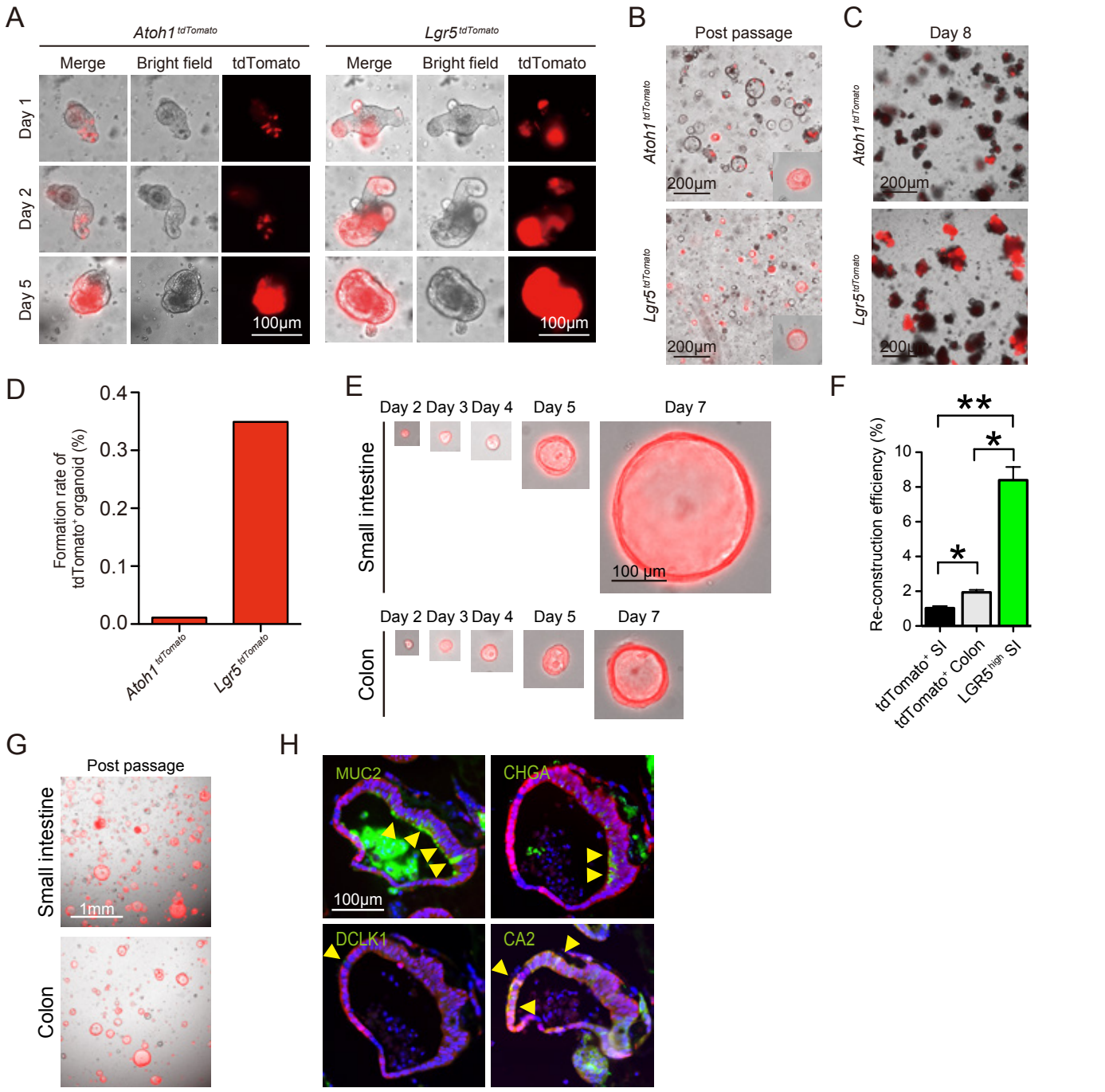

Figure S3. Related to Figure 3. ATOH1$^+$ IECs can form clonal ribbons *in vitro*.
(A) Formation of in vitro tdTomato$^+$ clonal ribbons (ATOH1$^+$ICRs) in small intestinal organoids established from *Atoh1*^{tdTomato} mice and *Lgr5*^{tdTomato} mice. Cre-mediated recomination was induced in the subject organoids in vitro, and the expression of tdTomato was examined on the following days. The expression of tdTomato shows a scattered pattern in the organoids of *Atoh1*^{tdTomato} mice on day 1 and day 2 but later occupies a large continuous area of the organoids (corresponding to ATOH1$^+$ICR) on day 5. Organoids from *Lgr5*^{tdTomato} mice already show a cluster of tdTomato$^+$ cells at the tip of the budding structure on day 1, followed by continuous extension of tdTomato$^+$ cells, which finally constitute nearly the entire organoid on day 5. (B) The tdTomato$^+$ organoids shown in (A) can reconstruct tdTomato$^+$ organoids after passaging. A magnified view of the re-constructed tdTomato$^+$ organoid is shown in the lower right corner. (C) A lower magnification view of the organoids labelled with tdTomato in vitro on day 8. The image shows a markedly low efficiency of whole-organoid labelling in organoids derived from *Atoh1*^{tdTomato} mice compared with those derived from *Lgr5*^{tdTomato} mice. (D) The efficiency of in vitro whole-organoid labelling was quantified on day 8. The number of organoids that were entirely labelled by tdTomato was normalized by the number of total organoids established during the experimental period. The presented data are the cumulative numbers acquired from four independent culture wells. (E) Single tdTomato$^+$ cells were isolated from the small intestine and the colon of *Atoh1*^{tdTomato} mice after 5-dose of RU486, and cultured to examine organoid re-construction. (F) Organoid re-construction efficiency of single, isolated tdTomato$^+$ IECs. Efficiency of small intestinal (SI) and colonic tdTomato$^+$ IECs derived from the *Atoh1*^{tdTomato} mice was compared to that of Lgr5^{high} cells derived from the *Lgr5*^{EGFP} mice. Data are expressed as the mean±SEM of 3 independent experiments. *$p < 0.05$, **$p < 0.01$. (G) Re-construction of tdTomato$^+$ organoids shown in (E) after passaging. (H) Multi-potency of a tdTomato$^+$ IEC confirmed by DBZ-mediated induction (5 μM, 3 h) of MUC2$^+$, CHGA$^+$, DCLK1$^+$, and CA2$^+$ IECs (green) in an organoid re-constructed from a single tdTomato$^+$ cell. Serial sections of an organoid at 4 days after DBZ treatment is shown.

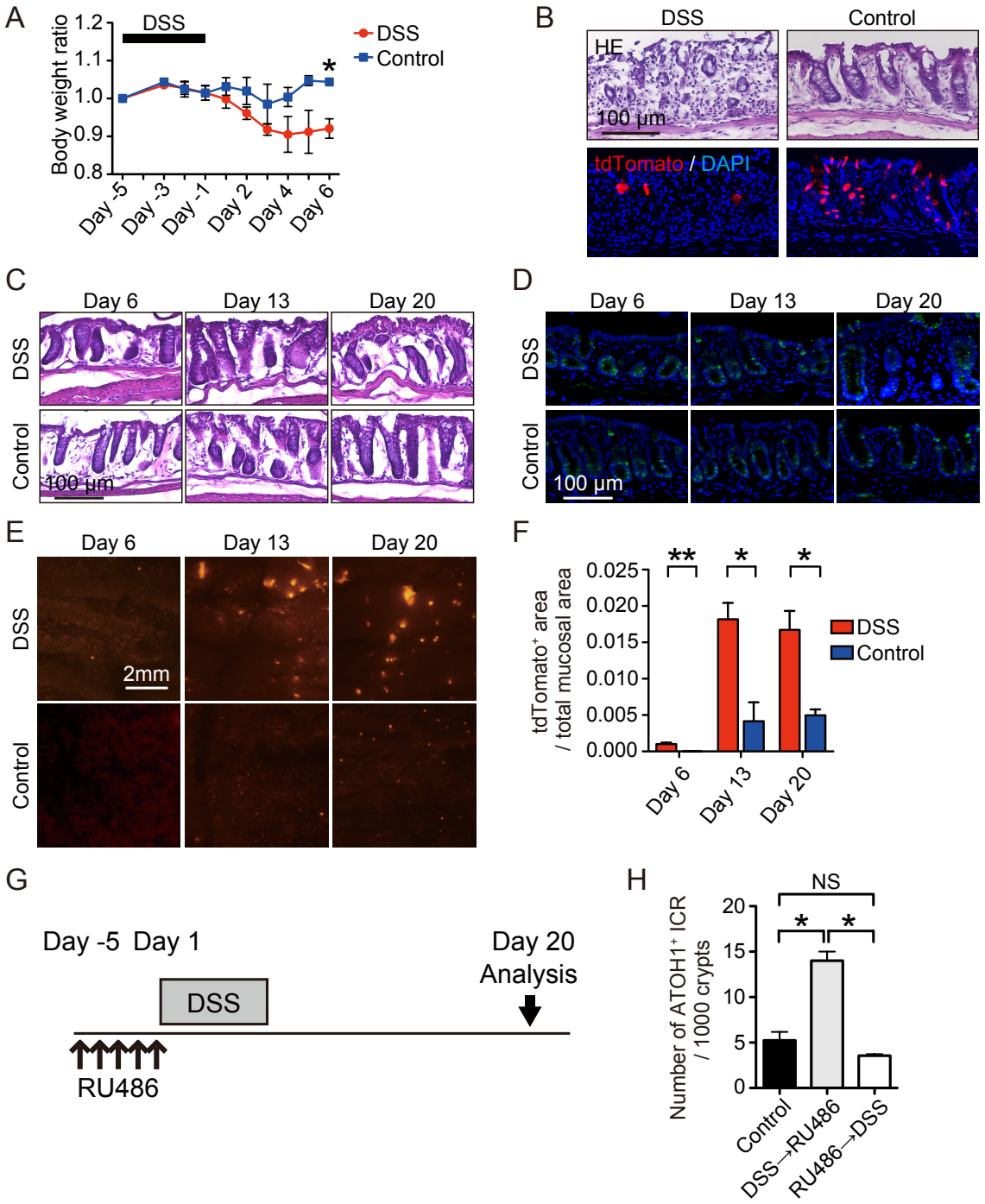

Figure S4. Related to Figure 4. Formation of ATOH1$^+$ ICR was enhanced by DSS induced colitis.
(A) Change in body weight during the experimental period, compared with the initial body weight. Data are expressed as the mean±SEM (n=3, biological replicate). * $p < 0.05$. (B) Representative rectal sections of DSS-colitis mice (DSS) and control mice (Control) at day 2. H&E staining (upper panel) show severe colitis in DSS-colitis mice. Only a few number of tdTomato$^+$ cells (lower panel) is labeled at this time period in DSS-colitis mice. (C) Representative H&E staining at each experimental period using rectal tissues of DSS-colitis mice (DSS; upper panel) and control mice (Control; lower panel). (D) Serial sections of (C), showing immunostaining of ATOH1 (green). (E) Fluorescence images of the tdTomato$^+$ area (red) in the rectum, examined at the designated experimental period. (F) Quantification of the tdTomato$^+$ area, as defined from the fluorescence view of the rectum. Data of DSS-colitis mice (n=3) and control mice (n=3) at each time point. Data are expressed as the mean±SEM. * $p < 0.01$, ** $p < 0.001$. (G) Experimental design to trace cell fate of pre-labeled Atoh1$^+$ cells in DSS-colitis mice. (H) Quantification of Atoh1$^+$ ICR generation in the distal colon of control mice (Control), post-labeled DSS-colitis mice (DSS→RU486) and pre-labeled DSS colitis mice (RU486→DSS). Data are expressed as the mean±SEM (3 independent experiments). * $p < 0.01$. NS, not significant.

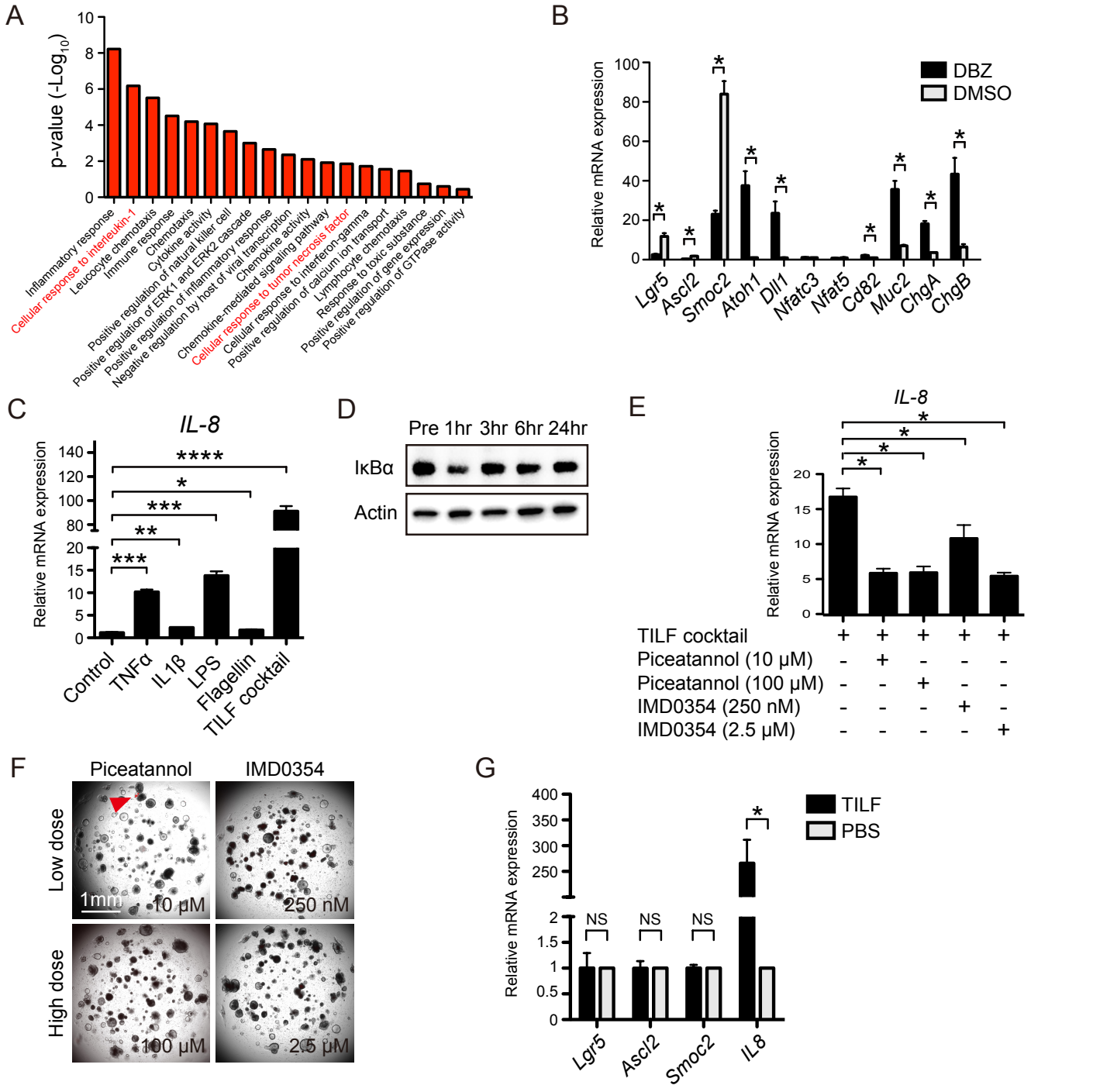

Figure S5. Related to Figure 5. Pro-inflammatory cytokines and bacterial components co-ordinately activate the NF-kB pathway to promote ATOH1^{+}ICR formation.

(A) Pathway analysis of the microarray data shown in Figure 5B ranked by p-values (-log10). (B) Quantitative RT-PCR analysis of colonic organoids subjected to DBZ-induced secretory lineage-differentiation (DBZ) or control treatment (DMSO) for 3 h. Organoids were collected 48 h after treatment. Data are shown as the mean±SEM (3 independent experiments). * $p < 0.01$. (C) Quantitative RT-PCR analysis of IL-8 expression in secretory lineage-differentiated colonic organoids treated with TNF-α, IL-1β, LPS, flagellin or a combination of all ligands (TILF cocktail). Data are shown as the mean±SEM(3 independent experiments). * $p < 0.05$, **$p < 0.01$, *** $p < 0.001$, **** $p < 0.0001$. (D) Immunoblot analysis of IkB-α expression in secretory lineage-differentiated colonic organoids treated with the TILF cocktail. (E) Quantitative RT-PCR analysis of IL-8 expression in secretory lineage-differentiated colonic organoids treated with the designated ligands or small molecule compounds for 24 h. Data are expressed as the mean±SEM (3 independent experiments). * $p < 0.01$. (F) In vitro ATOH1^{+} IEC lineage-tracing analysis of secretory lineage-differentiated colonic organoids. Organoids were treated with two different doses of piceatannol or IMD0354 for 48 h and examined for tdTomato expression using an epifluorescence microscope. The red arrowhead indicates an example of a tdTomato^{+} clonal ribbon formed in an organoid treated with a low dose of piceatannol. (G) Quantitative RT-PCR analysis of *Lgr5*, *Ascl2*, *Smoc2*, and *IL-8* expression in DBZ-untreated colonic organoids treated with the TILF cocktail or control (PBS). Data are shown as the mean±SEM (3 independent experiments. * $p < 0.01$. NS, not significant.

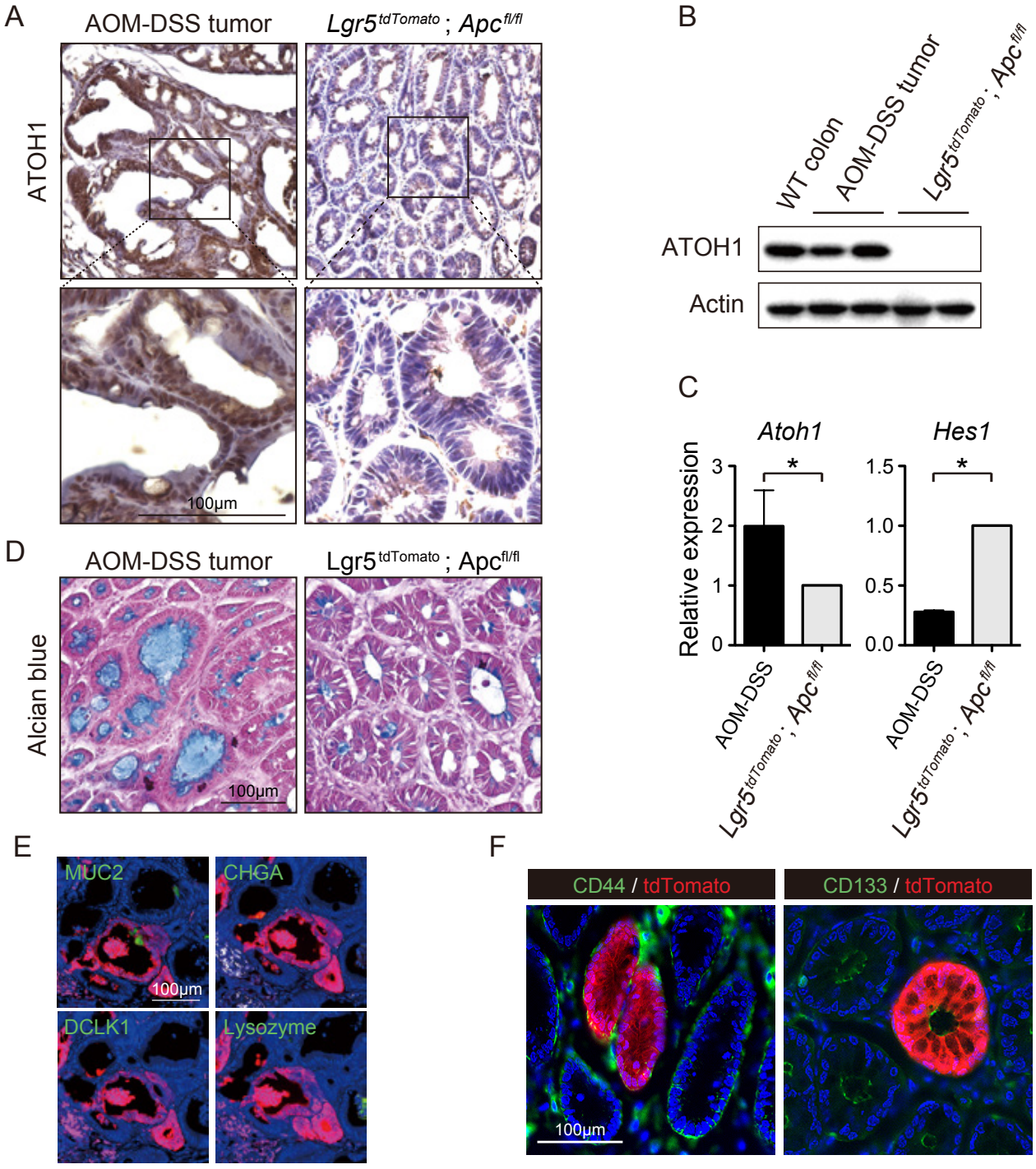

Figure S6. Related to Figure 6. AOM-DSS tumour cells exhibit a secretory lineage cell phenotype and can form ATOH1^{+}ICRs consisted of MUC2^{+}, CD44^{+} and CD133^{+} cells.

(A) Immunohistochemical analysis shows broad expression of Atoh1 in an AOM-DSS tumour, but its expression is nearly completely absent in the adenomas of *Lgr5^{tdTomato}; Apc$^{fl/fl}$* mice. (B) Immunoblot analysis of Atoh1 expression in the wild-type colon (WT colon), AOM-DSS tumours (AOM-DSS tumour), and the adenomas of *Lgr5^{tdTomato}; Apc$^{fl/fl}$* mice (*Lgr5^{tdTomato}*; *Apc$^{fl/fl}$*). The data show clear expression of Atoh1 in AOM-DSS tumours, but its expression is completely lost in the adenomas of *Lgr5^{tdTomato}; Apc$^{fl/fl}$* mice. Each lane represents the results obtained from an individual mouse. (C) Quantitative RT-PCR analysis of tumour organoids established from AOM-DSS tumours (n=3) or the adenomas of *Lgr5^{tdTomato}; Apc$^{fl/fl}$* mice (n=3). The data show significantly high expression of *Atoh1* and low expression of *Hes1* in AOM-DSS tumours compared with the adenomas of *Lgr5^{tdTomato}; Apc$^{fl/fl}$* mice. Data are shown as the mean±SEM. * $p < 0.01$. (D) Alcian blue staining reveals abundant expression of mucin (blue) in an AOM-DSS tumour but extremely low expression in an adenoma of an *Lgr5^{tdTomato}; Apc$^{fl/fl}$* mouse. (E) Double immunostaining of tumour ATOH1^{+}ICRs with various secretory lineage cell markers. ATOH1^{+}ICRs in the AOM-DSS tumours show clear co-staining for MUC2 (green) in a few tdTomato^{+} cells (red), but co-expression of CHGA, DCLK1 or Lysozyme was not observed. (F) Double immunostaining of tumour ATOH1^{+}ICRs with CD44 or CD133 (green).Representative data from two independent experiments.

Table S1. Primers Used for Genotyping, Related to Experimental Procedures Section

Gene	Forward primer	Reverse primer
Atoh1-CrePGR	5'-AGCGATGATGGCACAGAAG-3'	5'-GAAGTCAAGTCGTTGCTAAC-3'
Lgr5-EGFP-IRES-creERT2	5'-CTGCTCTCTGCTCCCAGTCT-3'	5'-ATACCCCATCCCTTTTGAGC-3'
		5'-GAACTTCAGGGTCAGCTTGC-3'
Apc-floxed	5'-GATGGGTCTGTAGTCTGGG-3'	5'-GGCTCAGCGTTTTCCTAATG-3'
ROSA26-tdTomato	5'-AAGGGAGCTGCAGTGGAGTA-3'	5'-CCGAAAATCTGTGGGAAGTC-3'
	5'-GGCATTAAAGCAGCGTATCC-3'	5'-CTGTTCCTGTACGGCATGG-3'
Apc-Min	5'-TTCCACTTTGGCATAAGGC-3'	5'-GCGATCCCTTCACGTTAG-3'
		5'-TTCTGAGAAAGACAGAAGTTA-3'

Table S2. Primary Antibodies Used for Immunohistochemistry, Related to Experimental Procedures Section

Antibody	Dilution	Origin	Catalog ID
anti-ATOH1	1:200	A kind gift from Dr. JE Johnson, UT Southwestern	
anti-HES1	1:60000	A kind gift from Dr. T Sudo, Toray Industry	
anti-MUC2	1:100	Santa Cruz Biotechnology	Sc15334
anti-CHGA	1:1000	Diasorin	SP-1
anti-DCLK1	1:100	Abgent	AP7219B
anti-Lysozyme	1:1500	DAKO	EC3.2.17
anti-Ki67	1:50	DAKO	TEC-3
anti-tdTomato	1:500	SICGEN Antibodies	AB8181-20
anti-CA2	1:100	Santa Cruz Biotechnology	Sc25596
anti-Villin	1:100	Merck Millipore	MAB1671
anti-CD24	1:500	Affymetrix eBioscience	140242
anti-DLL1	1:200	R&D Systems	AF5026
anti-CD44	1:50	BD Pharmingen	550538
anti-CD133	1:50	Affymetrix eBioscience	14-1331
anti-βcatenin	1:500	BD Bioscience	610153

Table S3. Primers Used for Quantitative RT-PCR, Related to Experimental Procedures Section

Gene	Forward primer	Reverse primer
Lgr5	5'-GGGCGTTAAGTCCACTGTGT-3'	5'-CGAACACCTGCGTGAATATG-3'
Olfm4	5'-TGGCCCTTGGAAGCTGTAGT-3'	5'-ACCTCCTTGGCCATAGCGAA-3'
Ascl2	5'-CTACTCGTCGGAGGAAAG-3'	5'-ACTAGACAGCATGGGTAAG-3'
Smoc2	5'- CAGGTCCAGTGTCACAGCTACAC -3'	5'- GGTCTTGTTCTGCCGACTCTTAAC -3'
Muc2	5'-GTCCGAAGTGTTACCCTGGA-3'	5'-CCAGGAGTGGAGAAGGTCAG-3'
ChgA	5'-GCAGAGGACCAGGAGCTAGA-3'	5'-CAGGGGCTGAGAACAAGAGA-3'
ChgB	5'- ACAGGAAGAAGGCAGACGAA -3'	5'- TCCTTCAGTGAAAGGCTCGT -3'
IL-8	5'- CGCCCAGACAGAAGTCATAG -3'	5'- TCCTCCTTTCCAGGTCAGTTA -3'
Dll1	5'-TGAGCCAGTCTTTCCTTGAA-3'	5'-AGACCCGAAGTGCCTTTGTA-3'
Nfatc3	5'- TTGTGCGTCAACTTCTGGTC-3'	5'- TAACTGAGGAGGAGCCTGGA -3'
Nfat5	5'- ACTGACCTGCCTTCTTGCAT-3'	5'-TTGACTGCAGCTGTTTACAGAAA -3'
Cd82	5'-TTGACTGCAGCTGTTTACAGAAA-3'	5'-AGCTGCCAAGAAACACCAGT-3'
Atoh1	5'-AGATCTACATCAACGCTCTGTC-3'	5'-ACTGGCCTCATCAGAGTCACTG-3'
Hes1	5'-TGCCTTTCTCATCCCCAACG-3'	5'-AGGTGACACTGCGTTAGGAC-3'
β-actin	5'-AGGTGACAGCATTGCTTCTG-3'	5'-AGGGAGACCAAAGCCTTCAT-3'

SUPPLEMENTAL EXPERIMENTAL PROCEDURE

Flow Cytometry Analysis

For cell preparation, resected intestinal or colonic tissues were soaked in cold PBS supplemented with 15 mM EDTA and 10 mM N-acetyl cysteine for 30 min. Crypts were isolated via pipetting and incubated in 10 ml of Advanced DMEM/F-12 (Thermo Fisher Scientific) supplemented with 13.5 U dispase Ⅱ (Thermo Fisher Scientific) and 8 mg DNase I (Sigma-Aldrich) at 37 °C for 10 min. The crypts were further dissociated into single cells using a buffer containing 5 ml of TrypLE express (Thermo Fisher Scientific). The cells were subsequently stained with an APC-conjugated anti-CD24 antibody (BioLegend, Cat. #101813) and subjected to analysis with a BD FACS Aria Ⅱ system. Results acquired from an isotype antibody served as control.

For *in vivo* EdU analysis, 100 μg of EdU (Invitrogen) was injected intraperitoneally into the mice, and the animals were analysed one hour after injection. Epithelial cells of the small intestine were then isolated and stained with Alexa Fluor 488-conjugated azide according to the manufacturer's protocol (Invitrogen, C35002). Stained results of corresponding epithelial cells collected from EdU untreated mice served as control.

Organoid Culture

Intestinal organoid culture was performed according to a previous report (Mizutani et al., 2012). For the *in vitro* induction of Cre-mediated recombination in organoids carrying the *Atoh1*$^{Cre\text{-}PGR}$ allele or the *Lgr5-EGFP-IRES-creERT2* allele, mifepristone (RU486, 1 μM) or 4-hydroxytamoxifen (4-OHT, 1 μM), respectively, was added to the medium for 24 h. For the secretory lineage differentiation of organoids, the organoids were placed in differentiation medium supplemented with EGF (50 ng/ml), Noggin (100 ng/ml) and dibenzazepine (DBZ, 5 μM) for 3 h and then returned to the original ENR medium for the following experimental period. The inflammatory ligands used to stimulate the secretory lineage-differentiated organoids are as follows: mouse recombinant TNF-α (100 ng/ml, Peprotech), mouse recombinant IL1-β (50 ng/ml, Sigma-Aldrich), lipopolysaccaride (LPS, 10 μg/ml, Sigma-Aldrich) and flagellin (10 ng/ml, Sigma-Aldrich). For the inhibition of NF-κB signalling, piceatannol (10 μM or 40 μM, Tokyo Chemical Industry) or IMD0354 (250 nM or 1 μM, Sigma-Aldrich) was added to the culture medium. For the evaluation of organoid re-construction efficiency by single isolated cells, tdTomato^{+} cells were sorted by BD FACSMelody (BD Biosciences), and seeded onto 96-well plates at a cell density of 1000 cell / well in 5 μl of Matrigel. Corresponding cells prepared from wild-type mice served as control for FACS gating. Cell culture was performed in 100 μl of standard culture medium, and examined for organoid re-construction every day.

DSS Colitis Model and AOM-DSS Tumour Model

The induction of colitis using dextran sodium sulphate (DSS) was performed as previously described (Okamoto et al., 2009). The daily change in whole body weight was recorded, and the mice were sacrificed on the designated experimental day.

The azoxymethane (AOM)-DSS tumour model was induced as previously described (Onizawa et al., 2009). Briefly, a single dose of AOM (10 mg/kg, Sigma Aldrich) was injected intraperitoneally on day 1, followed by three cycles of 3% DSS treatment on day 1 to day 5, day 22 to day 27 and day 51 to day 55.

To quantify the tissue surface area where tdTomato was expressed, fluorescent images of the rectum were captured using a stereoscope equipped with an RFP filter (CellSens, Olympus) and analysed using Image J software (version 1.48). After the arbitrarily cropped area was converted to an 8-bit image and binarized, the automatically traced areas (representing the tdTomato^{+} areas) were summed for each mouse and normalized based on the whole object area.

To quantify tdTomato^{+} tumour ducts (tumour Atoh1^{+} ICRs) or tdTomato^{+} area in AOM-DSS tumours, representative section of each tumour was subjected for analysis. For quantification of tumour Atoh1^{+} ICRs, total number of tumour ducts and the number of tumour Atoh1^{+} ICRs was counted for each subject section. For quantification of tdTomato^{+} area, section images were analysed by the Image J software, following the procedures described above.

Heterotopic Transplantation of AOM-DSS tumour organoids

AOM-DSS tumours that showed tdTomato expression were selectively resected under a stereoscope and used to establish primary tumour organoid lines. After 6 passages, the tumour organoids were collected and resuspended in ice-cold Matrigel. Organoids equivalent to 1×10^5 cells or 4×10^5 cells were then subcutaneously injected into BALB/cAJcl-*nu*/*nu* mice (8-week-old, male) using a 23-gauge needle (day 1). Normal colon organoids (1×10^5 cells) or HT29 cells (4×10^5 cells) were injected as a negative or positive control, respectively. Tumour size was measured at 7 and 14 days after transplantation. On day 15, the tumours were removed and fixed with 4% paraformaldehyde for immunohistochemical analysis.

Microarray Analysis

RNA extraction was performed using the RNeasy Mini kit (QIAGEN). The RNA samples were subjected to microarray analysis using a 3D gene chip (Toray Industry) as previously described (Fukuda et al., 2014) (Accession numbers; GSE81315 and GSE81451). Gene set enrichment analysis (GSEA) was performed using the Broad Institute software (version v2.2.2). The gene set files were obtained from MSigDB (M1999 and M1983). MA plot analysis was performed by using GraphPad PRISM software (version 5.0a, GraphPad Software). Pathway analysis was conducted using DAVID 6.8 (Huang et al., 2009).

RNAscope® In situ Hybridization

RNAscope® in situ hybridization analysis (RNAscope ISH) was performed by following the manufacturer's instructions. Briefly, 8 μ m tissue sections were subjected to antigen retrieval treatment (100℃, 5min) in Target Retrieval Agents (ACD, 32200). After dehydration, tissues were digested by protease treatment (40℃, 30 min, Protease III &Protease IV Reagents, ACD, 322340) and subsequently hybridized by gene-specific probes (Mm-Probe) at 40℃ for 2 h. Probes used for the present study are as follows: Lgr5, #312171; Ascl2, #412211; Atoh1, #408791-C2. Standard signal amplification was performed, and tissues were counterstained by 4′,6-Diamidine-2′-phenylindole dihydrochloride (DAPI). If needed, immunostaining procedures for tdTomato was added after the signal amplification.

Cell position number of $Lgr5^+Atoh1^+$ cells identified by RNAscope ISH was assigned by the methods described in the previous study (van Es et al., 2012).

Quantitative RT-PCR Analysis

RNA extraction, reverse transcription and quantitative PCR analysis were performed as previously described (Okamoto et al., 2009). The primers used for this analysis are listed in Table S3.

Immunoblotting Analysis

Standard immunoblotting was performed using the following antibodies; anti-Actin (1:5000, A5441, Sigma-Aldrich), anti-ATOH1 (1:1000, 21215-1-AP, Proteintech), and anti-IkBα (1:1000, #9242, Cell Signaling Technology).

Statistical Analysis

Unless otherwise indicated, the data are shown as the mean±SEM based on at least two rounds of independent experiments including over three biological replicates. The significance of these data was analysed using the unpaired two-sided Student's t-test. Significance was determined at $P < 0.05$. All statistical analyses were performed using GraphPad PRISM software (version 5.0a, GraphPad Software).

SUPPLEMENTARY REFERENCES

Fukuda, M., Mizutani, T., Mochizuki, W., Matsumoto, T., Nozaki, K., Sakamaki, Y., Ichinose, S., Okada, Y., Tanaka, T., Watanabe, M., Nakamura, T., 2014. Small intestinal stem cell identity is maintained with functional Paneth cells in heterotopically grafted epithelium onto the colon. Genes Dev. 28, 1752–1757. doi:10.1101/gad.245233.114

Huang, D.W., Sherman, B.T., Lempicki, R.A., 2009. Systematic and integrative analysis of large gene lists using DAVID bioinformatics resources. Nat Protoc 4, 44–57. doi:10.1038/nprot.2008.211

Mizutani, T., Nakamura, T., Morikawa, R., Fukuda, M., Mochizuki, W., Yamauchi, Y., Nozaki, K., Yui, S., Nemoto, Y., Nagaishi, T., Okamoto, R., Tsuchiya, K., Watanabe, M., 2012. Real-time analysis of P-glycoprotein-mediated drug transport across primary intestinal epithelium three-dimensionally cultured in vitro. Biochem. Biophys. Res. Commun. 419, 238–243. doi:10.1016/j.bbrc.2012.01.155

Okamoto, R., Tsuchiya, K., Nemoto, Y., Akiyama, J., Nakamura, T., Kanai, T., Watanabe, M., 2009. Requirement of Notch activation during regeneration of the intestinal epithelia. Am. J. Physiol. Gastrointest. Liver Physiol. 296, G23–35. doi:10.1152/ajpgi.90225.2008

Onizawa, M., Nagaishi, T., Kanai, T., Nagano, K.-I., Oshima, S., Nemoto, Y., Yoshioka, A., Totsuka, T., Okamoto, R., Nakamura, T., Sakamoto, N., Tsuchiya, K., Aoki, K., Ohya, K., Yagita, H., Watanabe, M., 2009. Signaling pathway via TNF-alpha/NF-kappaB in intestinal epithelial cells may be directly involved in colitis-associated carcinogenesis. Am. J. Physiol. Gastrointest. Liver Physiol. 296, G850–9. doi:10.1152/ajpgi.00071.2008

van Es, J.H., Sato, T., van de Wetering, M., Lyubimova, A., Nee, A.N.Y., Gregorieff, A., Sasaki, N., Zeinstra, L., van den Born, M., Korving, J., Martens, A.C.M., Barker, N., van Oudenaarden, A., Clevers, H., 2012. Dll1+ secretory progenitor cells revert to stem cells upon crypt damage. Nat. Cell Biol. 14, 1099–1104. doi:10.1038/ncb2581